Prevent or Cure—The Unprecedented Need for Self-Reporting Materials

Christina M. Geiselhart, Hatice Mutlu,* and Christopher Barner-Kowollik*

These are not the final page numbers!

Self-reporting smart materials are highly relevant in modern soft matter materials science, as they allow for the autonomous detection of changes in synthetic polymers, materials, and composites. Despite critical advantages of such materials, for example, prolonged lifetime or prevention of disastrous material failures, they have gained much less attention than self-healing materials. However, as diagnosis is critical for any therapy, it is of the utmost importance to report the existence of system changes and their exact location to prevent them from spreading. Thus, we herein critically review the chemistry of self-reporting soft matter materials systems and highlight how current challenges and limitations may be overcome by successfully transferring self-reporting research concepts from the laboratory to the real world. Especially in the space of diagnostic self-reporting systems, the recent SARS-CoV-2 (COVID-19) pandemic indicates an urgent need for such concepts that may be able to detect the presence of viruses or bacteria on and within materials in a self-reporting fashion.

From the Contents

1. Introduction

The growing demand on technologies in our daily lives requires evermore complex, innovative, and long-lasting materials. Therefore, scientists are taking inspiration from biological systems, which often possess the unique ability to sense, report and, if required, self-heal damages immediately, often relying on visual indication systems. Prominent examples are the bioluminescence of marine phytoplankton, falling leaves next to a color change from green to brown of plants in the absence of water, the red color of bleeding wounds, or the color change during the healing process of bruises. Indeed, the successful transfer of such properties to human-made materials has been reported and a plethora of bioinspired, stimuli-responsive smart materials has emerged.[1–8] These materials possess the ability to change their properties triggered by one or multiple stimuli,[9] for example, mechanical forces, temperature, pH, light, ultrasound, magnetic fields, or chemicals. Judiciously combining stimuli-responsive elements with suitable polymeric structures, fascinating smart materials have been developed, one important representative class being the self-healing materials.[10–16] Similar to biological organisms, such materials are able to repair damaged areas. The mechanisms of self-healing processes are thereby highly dependent on the initial design strategy. On the one hand, the mechanism can be autonomic, meaning the damage itself triggers the healing process by releasing healing agents embedded in for example, microcapsules, hollow (glass) fibers, or vascular systems at the damaged area. On the other hand, non-autonomic systems require an external trigger such as thermal, light, or chemical activation to induce for example (reversible) crosslinking or polymerization reactions to heal the damage.[17–22] Unfortunately, most of the self-healing processes are irreversible. Once the healing agent is released or the polymerization is carried out, it cannot be used again to heal further damage. Therefore, it is of critical importance to first report the existence and the

exact location of the damage before the actual healing process can take place. Thus, a fast detection of the damage is enabled and the healing process can be carefully monitored. Taking renewed inspiration from biological systems, the scope of stimuli-responsive materials has been expanded with the development of diverse self-reporting smart materials. Due to the advantages of such self-reporting properties for load-bearing materials, nanotechnology, biomedicine, or theranostics, we submit there is a critical need to review the self-reporting systems that have been developed based on the stimuli triggering the operating mechanisms (such as mechanical forces, temperature, pH, solvation, light, and chemicals).

[*] C. M. Geiselhart, Dr. H. Mutlu
Soft Matter Synthesis Laboratory
Institute for Biological Interfaces 3
Hermann-von-Helmholtz-Platz 1, 76344 Eggenstein Leopoldshafen (Germany)
E-mail: hatice.mutlu@kit.edu

C. M. Geiselhart, Dr. H. Mutlu, Prof. Dr. C. Barner-Kowollik
Macromolecular Architectures
Institute for Technical Chemistry and Polymer Chemistry (ITCP)
Karlsruhe Institute of Technology (KIT)
Engesserstrasse 18, 76131 Karlsruhe (Germany)
E-mail: christopher.barner-kowollik@kit.edu

Prof. Dr. C. Barner-Kowollik
Centre for Materials Science
Queensland University of Technology (QUT)
2 George Street, Brisbane, QLD 4000 (Australia)
and
School of Chemistry and Physics
Queensland University of Technology (QUT)
2 George Street, Brisbane, QLD 4000 (Australia)
E-mail: christopher.barnerkowollik@qut.edu.au

The ORCID identification number(s) for the author(s) of this article can be found under:
https://doi.org/10.1002/anie.202012592.

More specifically, the current Review focuses mainly on polymer-based smart materials that are able to indicate changes or damages immediately in a visible manner by changing color, fluorescence, or chemiluminescence. Furthermore, current challenges and limitations are highlighted along possibilities how they may be overcome by successfully transferring self-reporting research concepts from the laboratory to the real world. Finally, the (undervalued) potential of self-reporting materials as biomedical diagnostic tools will be discussed with regard to the latest SARS-CoV-2 pandemic.

2. Stimuli-Responsive Self-Reporting Polymeric Materials

Noting that the plethora of stimuli-responsive triggers is very broad, we herein critically focus on specifically selected representatives, which are summarized in Scheme 1. To aid the reader, we initially start with the most common self-reporting materials, that is, those featuring mechano-responsive properties. Subsequently, thermo-, pH-, solvation-, light-, chemically, and multi-stimuli-responsive systems will be discussed. Throughout, current issues as well as (future) possibilities are explored.

2.1. Mechano-Responsive Materials

As indicated above, mechano-responsive self-reporting materials (also known as self-sensing or self-monitoring)[23] are considered the most prevailing ones based on the multitude of studies and possible applications (e.g. load

bearing, high performance, aerospace, automobiles, biotechnology).[23–28] Mechanical forces apply to all different types of such materials, thus it is of critical importance to detect damages as early as possible to prevent catastrophic failures. In addition, preventive maintenance can be conducted more precisely (on demand) to increase the reliability and the lifetime of the materials at lower costs. Indeed, various techniques have been developed to report mechano-induced damage in a self-reporting manner. Generally, as illustrated in Scheme 1, the techniques are based on the incorporation of dye-filled capsules,[24,29–34] mechanophores,[35,36] fibers,[23,37,38] or sensor molecules[39–41] into composites, polymer matrices, or networks/hydrogels in order to mimic the nerve systems and tissues of biological organisms. Upon mechanical damage, the self-reporting output is triggered and made visible by changes in fluorescence, luminescence, or color.

For example, spiropyrans (SPs) have been incorporated into polymeric materials as the most investigated mechanophore to report microscale damages via distinct changes in color and fluorescence.[23,35,37,42–45] Mechanical forces lead to bond cleavage of the colorless SP, resulting in the isomerization into the fluorescent red colored merocyanine (MC, Scheme 1). For example, Silberstein and co-workers synthesized a high-performance SP polycarbonate, which responds to mechanical forces already at ambient temperature.[42] In another example, a SP-containing graft copolymer of rubbery poly(butyl acrylate) (PBA) as the backbone and glassy poly(methyl methacrylate) (PMMA) as comb side chains was synthesized, as illustrated in Figure 1 A.[43] The obtained polymer with SP (orange dots) as covalently incorporated connection between the PBA (blue lines) and the PMMA (red lines) exhibits green fluorescence ($\lambda_{em} = 530$ nm) due to

Christina M. Geiselhart received her M.Sc. in Chemistry from the Karlsruhe Institute of Technology (KIT, Germany) in 2017, where she performed her undergraduate studies. Currently, she is a PhD student at the KIT under the supervision of Dr. Hatice Mutlu and Prof. Christopher Barner-Kowollik, having spent research time both at the KIT and the Queensland University of Technology (QUT). Her research focuses on the development of macromolecular smart materials with self-reporting properties.

Hatice Mutlu, born in Bulgaria, studied Chemistry at Marmara University and Bogazici University. Subsequently, she obtained her PhD from the Karlsruhe Institute of Technology (KIT) in the group of M. A. R. Meier. After post-doctoral stays in the groups of J.-F. Lutz (ICS-CNRS, Strasbourg) and C. Barner-Kowollik (KIT), she currently works as a senior researcher at KIT. Her research interest spans from the synthesis of complex macromolecular architectures and functional polymers to the development of new polymer-forming reactions and novel conjugation chemistries with a particular focus on the design of novel sulfur-based and self-reporting materials.

Christopher Barner-Kowollik, Australian Research Council (ARC) Laureate Fellow, graduated in chemistry from Göttingen University, Germany, and joined the University of New South Wales in early 2000 rising to lead the Centre for Advanced Macromolecular Design in 2006 as one of its directors. He returned to Germany to the KIT in 2008, where he established and led a DFG-funded Centre of Excellence in soft matter synthesis. He moved to QUT in 2017 and established QUT's Soft Matter Materials Laboratory. His research achievements have been recognized by an array of national and international awards.
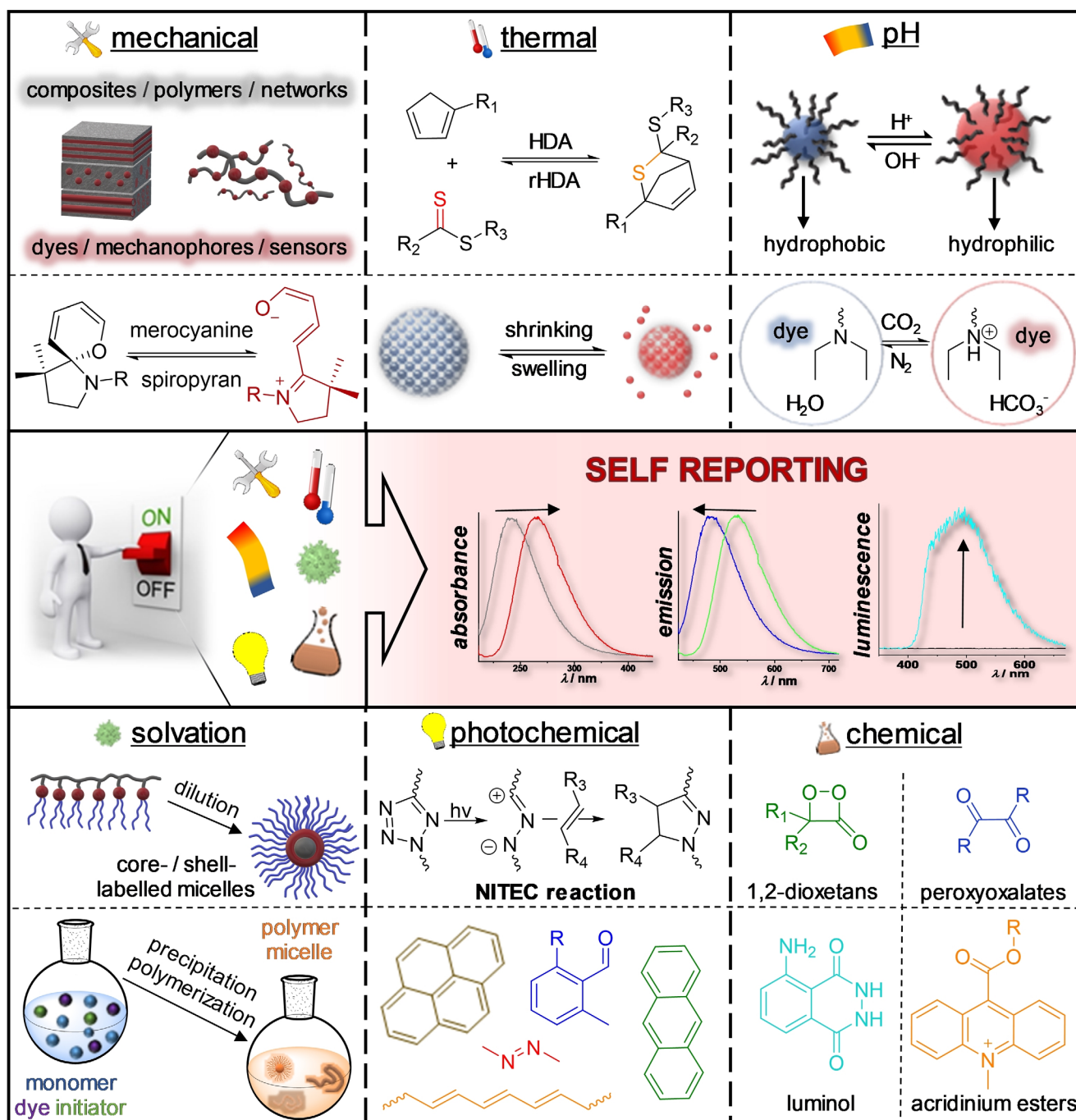
Scheme 1. Overview of stimuli (e.g. mechanical, thermal, pH, solvation, photochemical, and chemical) employed to switch on/off self-reporting properties of human-made materials, which are visualized by a change in color, fluorescence, or chemiluminescence. For each stimulus, selected representative examples are displayed, which will be further discussed throughout the current Review in the order shown above.

the fluorophore nitrobenzoxydiazole (NBD, green triangles) located in the PMMA side chains. Upon mechanical stimulus, the SP is converted into the MC derivative (red dots). Due to Förster resonance energy transfer (FRET), the green fluorescence of the NBD is quenched and the red fluorescence ($\lambda_{em} = 656$ nm) of the MC is observed. With increasing strain, the intensity of the green fluorescence decreases, while the intensity of the red fluorescence increases, until the material breaks down (Figure 1 B,C). The benefits of such a combina-

tion in one polymer are the high contrast between green and red fluorescence, the ability to monitor the change via laser scanning confocal microscopy, as well as the self-calibration of the ratiometric fluorescent signal. Thus, such SP-containing materials are promising candidates for sensor applications to self-report damages on the microscale. However, during the synthesis of mechanophores-containing polymers it has to be ensured that the initial high-performance or load-bearing properties of the desired materials are not depleted. Addi-
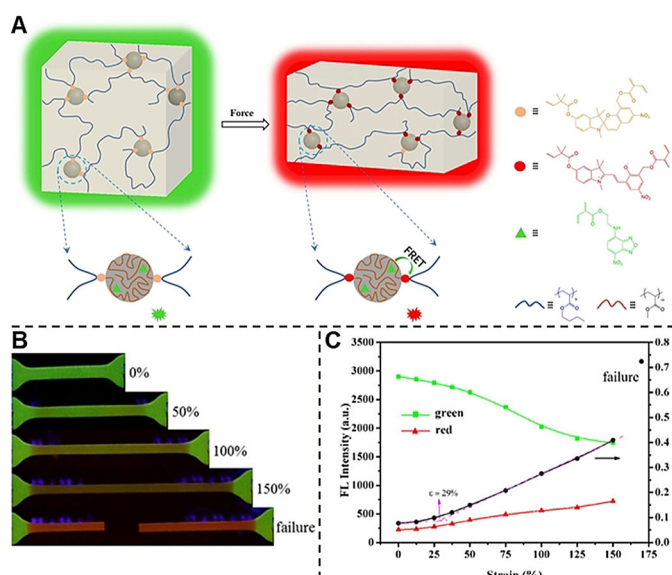
Figure 1. A) Schematic illustration of the PBA-SP-P(MMA-*co*-NBD) and its fluorescent color switch from green to red upon mechanical force. B) Fluorescence images of PBA-SP-P(MMA-*co*-NBD) under uniaxial tension, $\lambda_{ex} = 365$ nm. C) Fluorescence intensity between the green and red fluorescence emission peaks and the ratio between them vs. strain. Reprinted from ref. [43]. Copyright 2019 American Chemical Society.

Figure 2. A) Demonstration of the rotaxane-based mechano-responsive working principle. The rotaxane is equipped with anchor groups for incorporation into polymer chains (red), two stoppers (blue), and a fluorophore-containing cycle (gray/green) located around a suitable quencher (brown). Upon exposure to mechanical force, the fluorophore and the quencher are separated, switching on the fluorescence emission of the fluorophore. B) Molecular structure of the mechano-responsive rotaxane. C) Images of a PU film, whose fluorescence is turned on via stretching and turned off again by relaxation of the film. The films were irradiated at 365 nm and ambient illumination, respectively. Reprinted from ref. [48] with permission from ACS. (https://pubs.acs.org/doi/10.1021/jacs.7b12405. Further permissions related to the material excerpted have to be directed to ACS.)

tionally, mechanophores such as the spiropyrans, are responsive not only to mechanical stimuli, but also to for example, temperature or light (for more details see Section 2.7).[43,46,47]

One possible method developed to overcome such multi-responsiveness of mechanophores is the formation of supramolecular complexes. Weder and co-workers successfully applied rotaxanes as molecular shuttles in polyurethane elastomers, enabling the non-covalent encapsulation of mechanophores.[48] The working principle of such a rotaxane-based molecular shuttle and the respective molecular structure are displayed in Figure 2 A,B. A cycle containing the fluorophore (gray/green) is located around a suitable quencher (brown) with two stoppers (blue) and anchor groups (red) for incorporation into polymer chains (e.g. polyurethanes, PUs). Mechanical force separates the cycle with the fluorophore from the quencher and the fluorescence is turned on. Upon relaxation, the molecular shuttle returns to its former position around the quencher due to charge-transfer interactions, and the fluorescence is turned off again as displayed in Figure 2 C. These authors also showed that the turn-on/off process can be repeated several times (20 cycles tested) and is specific to mechanical stimuli, since no fluorescence was turned on at elevated temperatures. However, harsh conditions (temperatures > 150 °C or sonication) lead to a decomposition of the polymer films or irreversible cleavage of the mechanophores from the polymer. Nevertheless, the introduced concept of supramolecular shuttles is ideally suited to visualize mechanical forces in a reversible and specific manner. Further, the concept can possibly be fine-tuned by application of other supramolecular systems (e.g. catenanes, knots) and/or different chromophores to
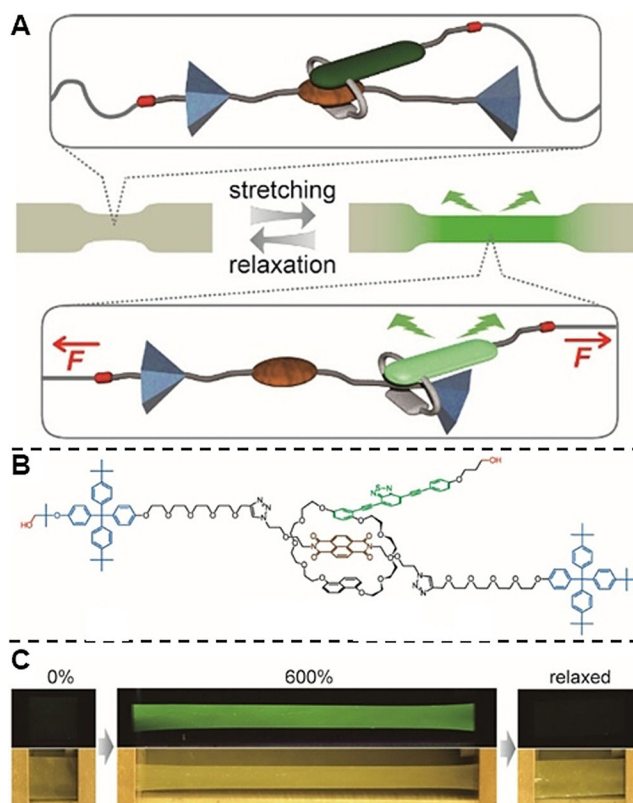
adjust the color and fluorescence emission, thus allowing the design of various kinds of mechano-responsive self-reporting systems.

Indeed, the concept of supramolecular complexes has been similarly exploited in the field of composites. Such materials provide light weight in combination with high mechanical strength and thus, they find application as structural components in for example, aircraft or automotive industry.[23,49] Therefore, it would be highly beneficial for composites to self-report damages and fatigue to prevent catastrophic failure. Analogous to the rotaxane-based molecular shuttle,[48] Das et al.[38] introduced a supramolecular host molecule, namely cucurbit[8]uril (CB[8]), into a carbon fiber epoxy (CFR) composite matrix. A highly fluorescent perylene monoimide (PER) as fluorophore and either an azobenzene (AZO) or dibenzofuran (DBF) derivative as quencher were simultaneously encapsulated by the CB[8], as shown in Figure 3. Via terminal amino groups, the fluorophore and the quencher were covalently cross-linked into the
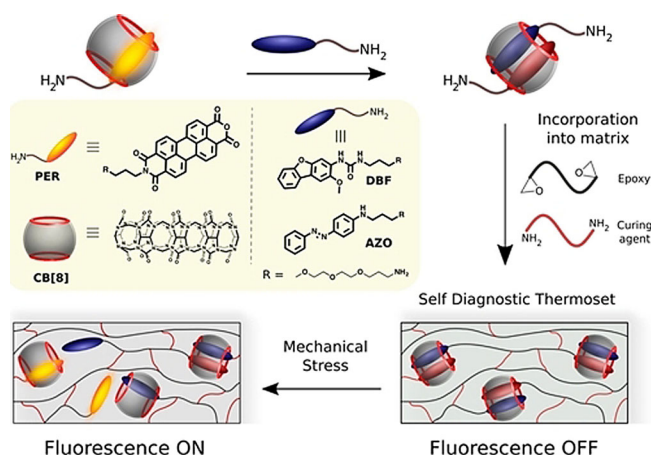
Figure 3. Operating mechanism of the cucurbit[8]uril (CB[8])-based damage-reporting CFR composites and the molecular structures of the applied host molecule (CB[8], gray/red), the fluorophore (PER, yellow), and the two quencher derivatives (azo and DBF, blue). Reprinted from ref. [38] with permission from ACS. (https://pubs.acs.org/doi/10.1021/acsapm.9b00694. Further permissions related to the material excerpted have to be directed to ACS.)

Figure 4. A) Dual-function microcapsule containing the tetraphenyl-ethylene (TPE) as AIEgen and hexamethylene diisocyanate (HDI)) as self-healing agent. B) Self-reporting and self-healing of the coating containing dual-function microcapsules. Pictures (C–E) of steel panels coated with C) pure E-epoxy coating, D) E-epoxy coating embedded with HDI microcapsules, and E) E-epoxy coating embedded with TPE/HDI microcapsules under white light. Pictures (F–H) of steel panels coated with F) pure E-epoxy coating, G) E-epoxy coating with HDI microcapsules, and H) E-epoxy coating embedded with TPE/HDI microcapsules under UV light. Reprinted from ref. [31]. Copyright 2020 ACS.

composite matrix. While no fluorescence is observed if both the fluorophore and the quencher are encapsulated in the CB[8], the fluorescence of the PER derivative is turned on upon mechanical force, which leads to a separation of the fluorophore and the quencher (Figure 3). Over 1000 cycles, no changes in fluorescence or stiffness were observed, starting slightly above 10000 cycles and above 100000 cycles a stiffness drop of 40% and fluorescence along the fibers were detected. Nonetheless, the supramolecular approach in the field of CFR composites allows the facile incorporation of self-reporting units into polymeric materials and can surely be transferred to other materials and suitable fluorophore–quencher pairs.

An alternative method to obtain mechano-responsive smart materials is the embedding of hollow microcapsules[24,29–33] or fibers[23,38] into the respective initial material. The microcapsules or fibers can be filled with dye molecules, which are released upon damage of their shell, thus indicating damaged areas. Not only does this method offer a broad versatility of applicable dye molecules, but it also enables the simultaneous incorporation of self-healing agents. If the stimuli-responsive container is broken by mechanical forces, the self-reporting as well as the self-healing agent are released. Clearly, such combined properties would be highly beneficial to prolong the lifetime and safety and to reduce warranty costs of human-made materials. Indeed, various materials with such combined self-healing and self-reporting properties have been reported, especially in the field of coatings.[34,40,50–54] Yang and co-workers for example synthesized microcapsules with both hexamethylene diisocyanate (HDI) as self-healing agent and a tetraphenylethylene (TPE) derivative as self-reporting agent (Figure 4A).[31] Embedded into polymer coatings, these microcapsules break upon exposure to mechanical forces and release their content. The HDI solution initiates the self-healing process with no need for any additional catalyst, and the damaged areas can be monitored under UV light by the blue fluorescence of the
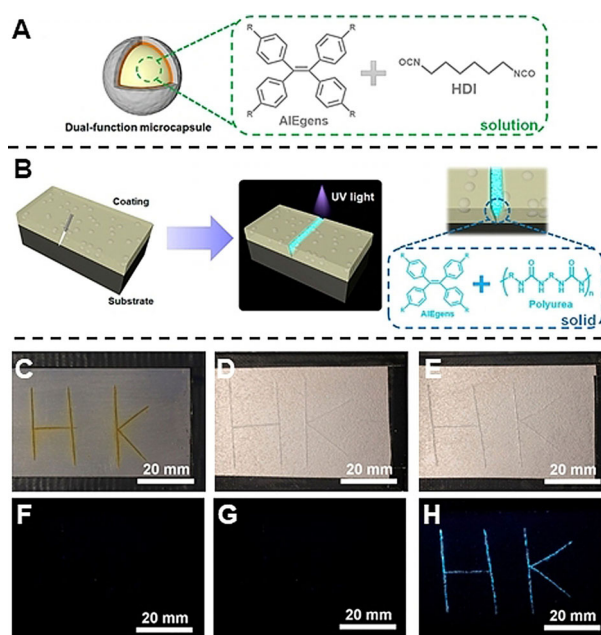
TPE, as illustrated in Figure 4B. To prove the applicability of the dual-function microcapsules as self-reporting and self-healing coating material, steel panels were coated with pure epoxy resin (Epolam 5015, E-epoxy), E-epoxy embedded with microcapsules containing only the self-healing HDI solution, and E-Epoxy embedded with the dual function microcapsules. Subsequently, the coated steel panels were damaged with a sharp blade and soaked in 10 wt% NaCl aqueous solution. Figure 4C–E clearly shows a strong corrosion of the steel panel coated only with the pure E-epoxy (Figure 4C), while the steel panels coated with HDI- (and TPE-)containing microcapsules show almost no corrosion (Figure 4D,E). Under illumination with UV light, a strong fluorescence in the repaired area is exclusively obtained for the steel panel coated with the dual-function microcapsules (Figure 4F–H). Similarly, Song et al. reported the synthesis of microcapsules with a single aggregation-induced emission (AIE) fluorophore, that provides different fluorescent colors in the liquid (intact) or in the solid state (damaged).[32]

There exist many more related dual-function smart mechano-responsive materials, clearly indicating the importance, actuality and demand to further investigate such materials. Yet, more research needs to be conducted to improve the contrast between the intact and damaged parts and to make such materials suitable and affordable for industrial applications. Particularly, the reversibility and the

These are not the final page numbers! ↗↗

selectivity of the self-reporting output needs to be considered. As indicated above, the mechano-responsive behavior based on the cleavage of covalent bonds (e.g. the isomerization of SPs) can be triggered by multiple stimuli. Microcapsules or fibers, on the other hand, are able to report damages only once, since they break upon mechanical deformation and the self-reporting component is released. Therefore, the most promising strategy is perhaps the supramolecular approach based on non-covalent interactions, since they provide selective and recyclable self-reporting response towards mechanical forces. Extensive research into such materials may help to prevent accidents due to material failure or catastrophes such as the collapse of the motorway bridge in Genoa, Italy in August 2018 in the future.[55–57]

2.2. Thermo-Responsive Materials

While intensive research has been conducted to design smart self-reporting (and self-healing) mechano-responsive materials, polymeric materials and their characteristics can also be influenced by temperature. Changes in temperature can lead to a change in for example, the aggregation state, color, or brittleness, thus it is of the utmost importance to consider the impact of the temperature and how the material adapts to alterations.[58–61] Indeed, various thermo-responsive materials have been developed by synthesizing composites/polymers/hydrogels (e.g. poly(N-substituted (meth)acryl-amide)s, polyoxazolines, polyethers, polycaprolactones, poly-phosphazenes, or polypeptides),[62] which possess a lower or upper critical solution temperature (LCST or UCST, respectively), thermochromic moieties, a temperature-dependent self-assembly-behavior, or incorporate thermo-responsive additives such as (leuco-)dyes, quantum dots, or inorganic thermochromic complexes.[61]

Especially in the context of energy saving and solar modulation, thermo-responsive materials are of key interest.[63–70] Heating and cooling systems in any vehicle, storage place, or indoor space require high amounts of energy, cause environmental problems (toxic cooling substances, pollution)[71,72] or may result in health issues (dry skin, headaches, colds).[73,74] Therefore, smart thermo-responsive glazing systems along window coatings have been developed.

For example, Lin and co-workers mixed dodecanedioic acid (DDA) with glycerol to obtain a cross-linked polyester network (PGD) as illustrated in Figure 5 A,B.[64] The material contains both amorphous domains (the cross-linked PGD network) and semi-crystalline domains (non-cross-linked DDA side chains, Figure 5 B). Below the transition temperature (39.1 °C), the two domains possess different refractive indices (RI) and thus the material is translucent (left side in Figure 5 C). Above the transition temperature however, the non-cross-linked DDA units melt and the RI of the semi-crystalline domain becomes similar to the one of the amorphous domains. As a result, the material becomes transparent (right side in Figure 5 C). Additionally, the mechanical strength of PGD-coated glass was up to 10 times higher than for bare glass, depending on the thickness of the coating.
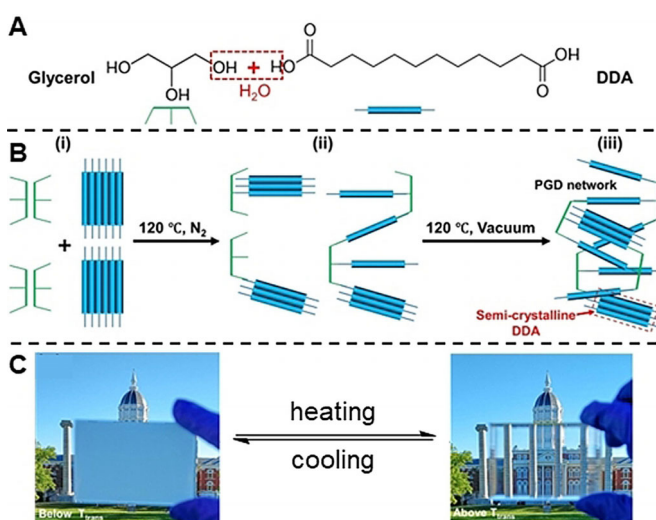

Figure 5. A) Esterification of glycerol and dodecanedioic acid (DDA). B) Polycondensation and network formation of glycerol and DDA. C) Photographs of PGD-coated glass below (left) and above (right) the transition temperature. Reprinted from ref. [64], Copyright 2019 American Chemical Society.

On the other hand, a polyurethane (PU)-based ionogel was synthesized changing from transparent to translucent properties upon heating.[65] The ionogel consists of ionic liquids (IL) cross-linked with poly(propylene oxide) (PPO) via urethane chemistry. At ambient temperature, the ionogel is homogeneous and transparent, while elevated temperatures lead to a phase separation between the IL and the PU network, which results in light scattering and a reduction of the optical transmittance. By changing the composition of the IL, the transition temperature range could be tuned from below zero to > 100 °C with a gradual change in the transparency below and above the transition temperature. In an experimental setup of a model house with either a smart ionogel window or a conventional float glass window, the house with the ionogel window showed a reduced temperature of 20 °C compared to the conventional one. Additionally, the optical properties were further adjusted by incorporating organic dye molecules or plasmonic nanoparticles into the ionogel.

Similar phase transitions from transparent to translucent (or vice versa) were obtained in liquid-crystal siloxane polymers,[66] polyacrylamide hydrogels,[67,68] nanoparticle–polymer composites,[69] or dynamic porous silicon films.[70] Clearly, these materials are promising for future developments of smart, thermo-responsive systems for solar control coatings and windows, displays, or sensors with tunable thermal and optical properties.

Another application field for thermo-responsive materials is biomedicine and drug delivery.[75–79] For example, inverse optical particles obtained from poly(N-isopropylacrylamide) (pNIPAM) hydrogels show thermo-responsive characteristics.[80] Depending on the temperature, the particles shrink or swell accompanied by a color change form red to blue, as depicted in Figure 6 A, making them an ideal system for drug delivery applications. The particles provide macropores for
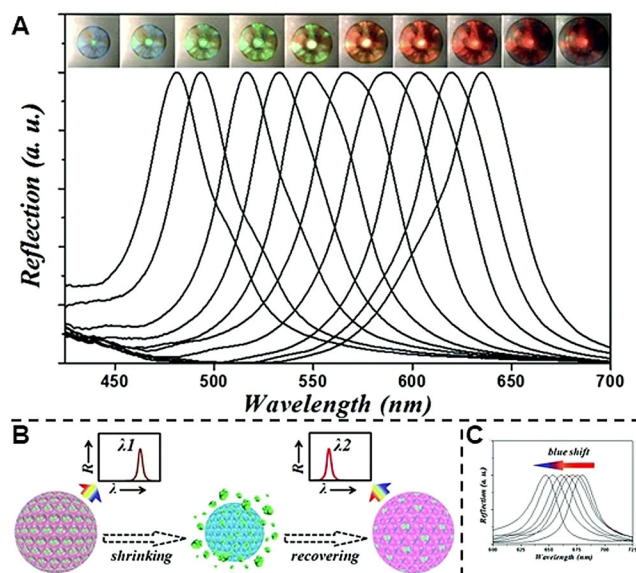
Figure 6. A) Reflection images and spectra of pNIPAM hydrogel inverse opal particles during a dynamic temperature decrease process. B) Schematic representation of the particles during drug release. C) Reflection spectra of a particle at different cycles of triggered drug release. Reproduced form ref. [80] with permission from the Royal Society of Chemistry.

active drug loading, which can be precisely released by adjusting the temperature. Intriguingly, the drug release was fine-tuned, hence allowing for the regulation of the drug delivery and the recovery of the initial particles (Figure 6B). Since the reflection spectra of the drug-loaded particles shown in Figure 6C also reveal a blue shift from approx. 650 to 475 nm during the release process, the system becomes self-reporting and enables the in situ monitoring of the drugs.

Yet, further research is required to improve the drug loading, since the loading mainly functions for macromolecular drugs. Further, the temperature applied for the drug release lays between 45 and 55 °C, which needs to be decreased in order to facilitate in vivo applications. Nevertheless, combined with the non-toxicity and biocompatibility of pNIPAM, such inverse opal particles are promising for biomedical applications, especially for drug delivery systems.

Furthermore, thermo-responsiveness has proven to be a powerful tool in the field of bonding/debonding on demand polymeric materials.[81–83] The required bonding or debonding process can be readily induced by heating or cooling of the material. Certainly, a significant temperature difference is required to avoid undesired bonding/debonding by coincidence rather than on demand.

One of the most attractive reactions fulfilling such criteria is the hetero Diels–Alder (HDA) reaction, since various dienes and dienophiles are available to precisely tune the range of the thermo-responsiveness.[84–86] For example, cyclopentadienes and dithioesters are able to undergo a HDA reaction at ambient temperature, while the reaction can be reversed by increasing the temperature, for example, in the range of 30–140 °C. Therefore, a HDA-based monomer has been synthesized from a methacrylic cyanodithioester and

a cyclopentadiene, which allowed subsequent incorporation of pyrene as fluorophore.[87] By copolymerizing this HDA monomer with 2,2,6,6-tetramethylpiperidine-4-yl methacrylate in a free radical polymerization, the statistical copolymer P1 with strong fluorescent properties is obtained, as illustrated in Figure 7. Upon oxidation with *meta*-chloroperbenzoic acid (mCPBA), the fluorescence is quenched due to conversion of the piperidine moiety to a nitroxide radical, yielding the profluorescent copolymer P2 in Figure 7. Finally, the debonding process is initiated by heating of the polymer to 90 °C, when the HDA unit is released and the fluorescence of the pyrene is recovered in such an intensity that it can be readily observed with the naked eye (Figure 7). Hence, a self-reporting thermo-responsive polymer system is obtained based on HDA chemistry combined with spin fluorescence silencing, which ideally lends itself to molecular sensing.

In a different, yet related example based on the HDA chemistry, polymeric methacrylic (HDA-PMA)[88] or dimethylcarbonate (HDA-PC)[89] networks have been formed, consisting of a di- or tricyclopentadiene (Di-/TriCp) and a phosphoryl dithioester (PDT), displayed in Figure 8 A,B. While the bonding process for the network formation is carried out at ambient temperatures to avoid early cleavage of the HDA moieties, the debonding process is conducted at elevated temperatures between 30 and 140 °C. The processes were reversible in several cooling/heating cycles, as evident from UV/Vis (Figure 8C) and ¹H NMR (Figure 8D) analysis. During three heating/cooling cycles from 20 to 100 °C, similar absorbance spectra are recorded (Figure 8C), clearly evidencing the reversibility of the (de-)bonding process. Specifically, the resonance changes associated with the cyclopentadienyl moiety (6.5–6.5 ppm) and the HDA unit (5.85–5.6 ppm) in the ¹H NMR spectra (Figure 8D) support the successful (de-)bonding on demand properties. In addition, the (de-)bonding process can be readily followed by the naked eye. While the bonded HDA-PC network is solid and slightly yellow, the cleavage of the PDT moiety during the retro-HDA results in a liquid, highly red colored material due to debonding of the polymer chains and the absorption of the
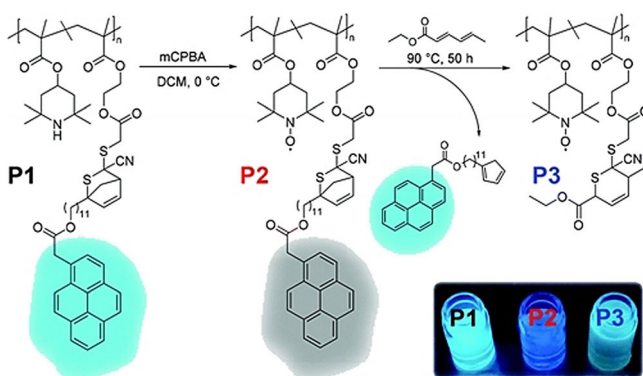

Figure 7. Statistical copolymer P1, whose strong fluorescence is silenced after oxidation with mCPBA, yielding the profluorescent copolymer P2. Upon heating of P2, the debonding of the HDA unit is initiated and the fluorescence of the pyrene units is recovered. Reproduced from ref. [87] with permission from the Royal Society of Chemistry.
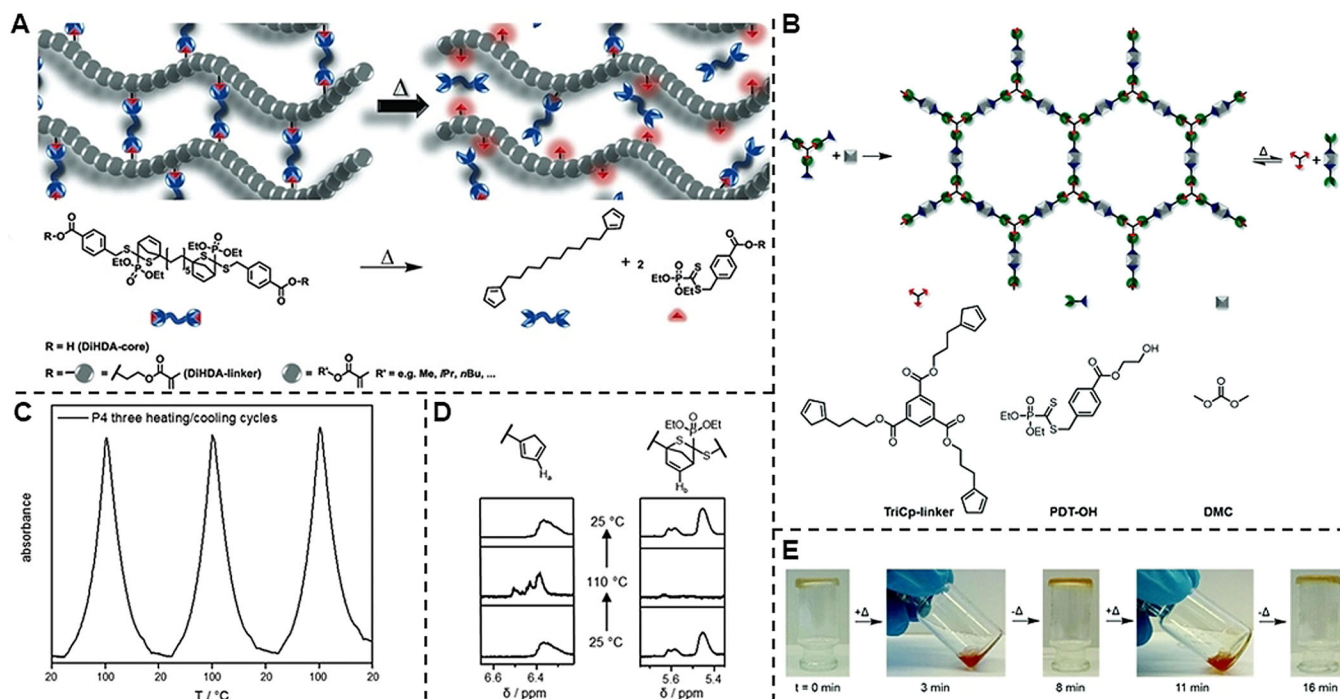
Figure 8. Schematic representation of A) the HDA-PMA and B) HDA-PC networks, enabling the bonding/debonding on demand process based on the thermo-responsive (retro) HDA reaction, which is exemplarily shown for A) the methacrylic network. C) UV/Vis analysis of the HDA-PC network during three heating/cooling cycles from 20 to 100 °C ($\lambda = 530$ nm, heating/cooling rate $= 5$ °C min^{-1}). D) Region of interest in the ¹H NMR spectra of the cyclopentadienyl moiety on the left (6.5–6.4 ppm) and the resulting HDA unit on the right (5.85–5.6 ppm). E) Behavior of the HDA-PC network upon 2 heating ($+\Delta$, 120 °C) and 2 cooling ($-\Delta$, 25 °C) cycles. Reproduced from ref. [88], copyright © 2016 The authors, Wiley-VCH GmbH, Weinheim (A) and from ref. [89] published by the Royal Society of Chemistry (B–E).

formed C=S double bond, as depicted in Figure 8E. Since the properties and thermo-responsiveness can be fine-tuned depending on the polymerization process, addition of suitable comonomers, or different HDA pairs, such materials disclose promising application possibilities in various fields, for example, adhesives or medical technologies.

2.3. pH-Responsive Materials

The discussion regarding the above pNIPAM particles already suggests the importance of particle sizes and their swelling/shrinking behavior. However, the change of the particle size and state does not have to be solely induced by temperature, but can also be caused by pH changes.[90–93] Especially in the fields of drug delivery, bio- or nanotechnology, pH-responsive materials are of high interest since certain pH values are characteristic for either healthy (pH $\approx$ 7.4) or diseased tissue (pH < 7).[94–96] Therefore, particles with different fluorescent characteristics in their swollen or shrunken state facilitate the reporting of environmental changes depending on the pH values.

Wang and co-workers took advantage of such particles to monitor the microenvironmental pH in the endocytosis process for the transportation of nanomedicines.[97] A bis-(pyrene) (BP) moiety was conjugated with poly(amino ester)s (P) terminated by cyclic peptides to build a pH-sensitive nanocarrier (P-BP) as displayed in Figure 9A. The BP

enables the formation of J-type nanoaggregates through hydrophobic and π–π interactions in water, while the tertiary amine groups of P (blue arrow in Figure 9A) ensure the reversible protonation and thus the shrinking and swelling of the particle depending on the pH value. The cyclic peptide units at the chain ends enable the targeted cell uptake. At neutral pH, the P-BPs were self-assembled into nanoparticles with a hydrophilic shell (P) and a hydrophobic core (BP), which enabled the encapsulation of Nile Red (NR) to visualize the self-assembly via red fluorescence emission (Figure 9B). In the presence of NR, the fluorescence of BP is quenched due to Förster resonance energy transfer (FRET) between NR and BP. If the pH value decreases from 7.4 to 5.0, the protonation of the tertiary amine groups in the polymer chains induces swelling of the particles (from 41.7 to 183.2 nm). The NR is released and its fluorescence is quenched due to aggregation in water, while simultaneously the fluorescence of the BP moieties is turned on due to a breaking of the fluorescence-quenching J-type nanoaggregates in the shrunken state and thus, the elimination of the FRET effect. Thus, the changes in the fluorescence emission allow the in situ monitoring of microenvironmental pH values, which is especially useful in the field of biology and medicine for the precise development of nanomedicine, for example, for the treatment of (benign/malignant) cancer diseases. By loading pharmaceutical active molecules into pH-responsive nanoparticles, these entities are exclusively released upon uptake of diseased cells within the range of
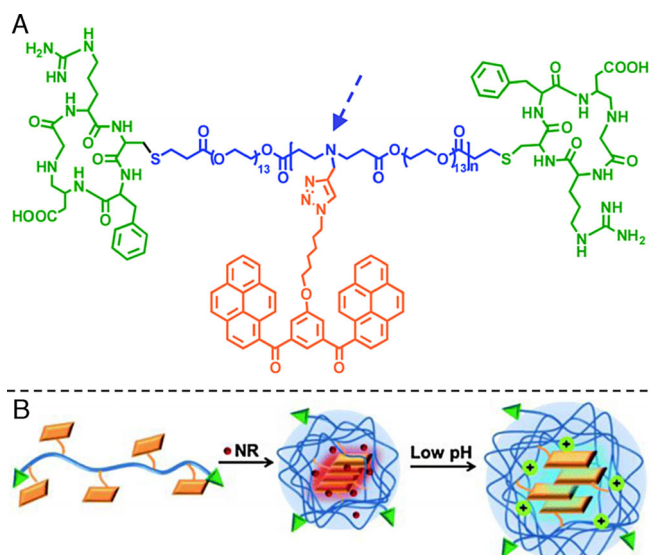
Figure 9. A) Nanocarrier P-BP with poly(amino ester)s as the pH-responsive backbone (blue) terminated by cyclic peptides (green) to enable cell uptake and a conjugated bis(pyrene) (BP, orange) as fluorophore. B) Self-assembly of P-BP into nanoparticles with a hydrophilic shell (P) and a hydrophobic core (BP). Encapsulation of Nile Red (NR) leads to a red fluorescence, which is blue shifted at lower pH values due to the elimination of the FRET effect. Reprinted from ref. [97] with permission from the Royal Society of Chemistry.

suitable pH values. Thus, in contrast to conventional nanomedicines without pH-responsive properties, the selectivity, sensitivity, and efficiency of the active compounds were improved, while simultaneously unwanted cellular cytoxicity and side effects may be reduced.[98–102]

Similarly, aminobromomaleimide (ABM) has been incorporated into particle cores as fluorophore to probe the core hydrophobicity.[103] The particles were synthesized via emulsion copolymerization of a hydrophilic shell-forming monomer (oligoethylene glycol methacrylate, OEGMA), a hydrophobic core-forming segment (N,N-diethylaminoethyl methacrylate, DEAEMA), and the respective fluorescent ABM monomer, represented in Figure 10A. In the presence of CO_2, the pH decreases due to the dissociation of CO_2 into HCO_3^-, CO_3^{2-}, and H^+, which leads to the protonation of the amine moieties and thus, to a swelling of the particles. The increased hydrophilicity of the swollen particles results in the quenching of the former fluorescence, allowing a facile observation of the swelling process via fluorescence measurements (Figure 10B) and DLS analysis (Figure 10C). Importantly, the swelling can be reversed by simply purging the solution with N_2 and thus the fluorescence is turned on again. However, the reversibility is highly dependent on the density and stability of the shell. Although the fluorescence emission intensity adjusts to a rather constant change after several purging cycles with CO_2/N_2 as evident from Figure 10D, the hydrodynamic diameter shows drastic fluctuation (e.g. up to 150 nm difference between two N_2 purging cycles, Figure 10E). Therefore, intensive research needs to be conducted to improve the stability of the particles, for example by alternating the monomers for the emulsion copolymerization or increasing the amount of crosslinker. Nevertheless, such self-reporting pH-responsive materials promise great potential for applications in sensor technology and biomedicine.

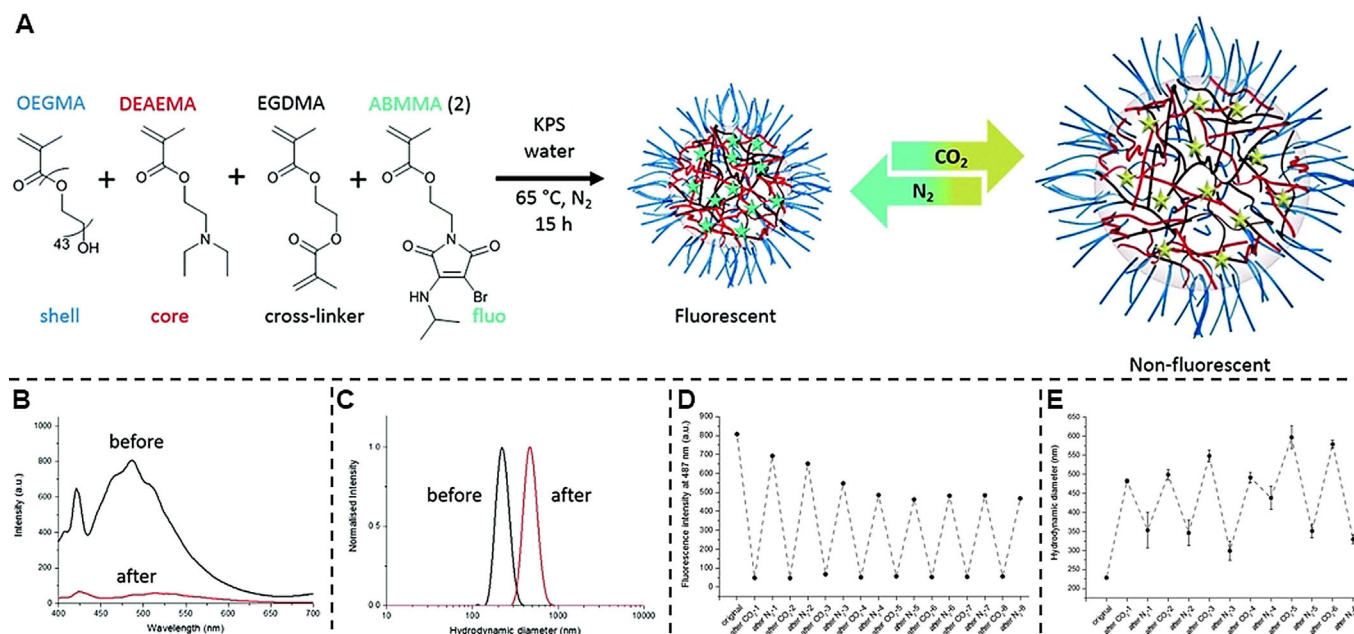**Figure 10.** A) Synthesis of PDEAEMA particles via emulsion polymerization and their pH/CO_2-responsive behavior. B) Fluorescence spectra and C) DLS analysis of PDEAEMA particles before and after the first CO_2 purge. D) Fluorescence intensity at 487 nm and E) hydrodynamic diameter of the PDEAEMA particles in deionized water after each gas purge. Reprinted form ref. [103] published by the Royal Society of Chemistry.

2.4. Solvation-Responsive Materials

In addition to temperature and pH as stimuli for self-reporting properties, polymer nanoparticles and micelles have been developed that respond to solvation stimuli. Upon dilution, the self-assembly of copolymers, decorated with both hydrophilic and hydrophobic segments, into micelles is induced. Similar to the previously introduced pH-responsive materials, such self-assembling polymers are of key interest in the biomedical field, especially for imaging and sensing.[104–106] Thus, amphiphilic block copolymers have been developed with integrated fluorophores and dye molecules, to allow the self-reporting monitoring of assembly and encapsulation behavior. Most importantly, the synthetic routes have been optimized so far to not only enable the covalent attachment of the fluorophore to the materials, but also to position the fluorophore variably, either in the micelle core or shell. This variability was achieved by synthesizing copolymers poly(tri-ethylene glycol acrylate)-*b*-poly(*tert*-butyl acrylate) (P-(TEGA)-*b*-P(tBA)) with a dithiomaleimide (DTM) fluoro-phore (green) either in the core forming (P(*t*BA)) block (red, CLP) or the shell forming (P(TEGA)) block (blue, SLP) by reversible addition–fragmentation chain-transfer (RAFT) polymerization.[106] The structures of the obtained CLP and SLP are displayed in Figure 11 A. Direct dissolution in water afforded the desired micelles, either core-labeled (CLM) or shell-labeled (SLM), as illustrated in Figure 11 B. Indeed, the

position of the fluorophore plays a critical role regarding the fluorescent properties. While the DTM fluorophore in SLMs suffers from solvent quenching effects, good protection of the chromophore is provided in the predominantly solvent-free core of CLMs. Therefore, CLMs show a brighter emission and a longer fluorescence lifetime in the micellar state than the SLMs. Furthermore, the CLMs could be used to self-report the presence of fluorescent hydrophobic guest molecules such as Nile Red (NR) due to the FRET effect (Figure 11 C. On uptake of the guest molecule into the core of the CLMs, the DTM emission at 515 nm was quenched, while the emission of NR at 610 nm was enhanced (the emission being higher than for non-labeled micelles with only NR present), as can be clearly seen in the emission spectra in Figure 11 E. The latter is only possible when the two fluorophores are in close proximity (generally < 4 nm), which proves that the FRET occurs in the core of the CLMs. However, in the presence of a hydrophilic guest molecule, for example, Rhodamine B (RhB), no FRET is observed (Figure 11 F), indicating that the RhB is not encapsulated into the micelle core, as illustrated in Figure 11 D. Thus, the CLMs not only self-report on the formation of the micelles upon dilution of the polymer, but also on the presence (or absence) of small guest molecules by simply measuring the changes in the fluorescence emission, which is of particular interest for drug delivery applications. Moreover, the fluorescent properties can be readily tuned by carefully choosing the substituents of the maleimide-based
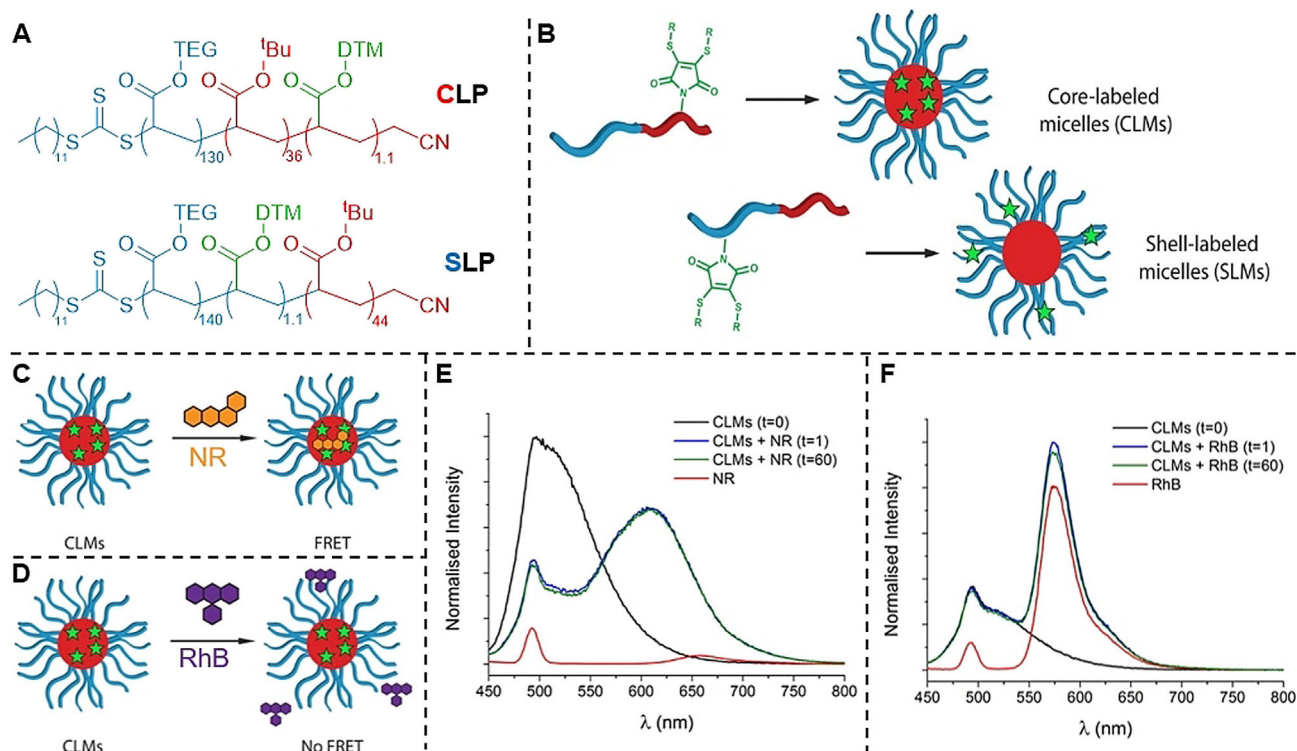
Figure 11. A) Structures of the core-labeled (CLP) and shell-labeled (SLP) block copolymers. B) Synthesis strategy for core-labeled micelles (CLMs) and shell-labeled micelles (SLMs). C) Interactions between CLMs and Nile Red (NR). D) Interactions between CLMs and Rhodamine B (RhB). Emission spectra (E–F) of CLMs at $t = 0$, 1, and 60 min after addition of E) NR (NR in water/0.1% 1,4-dioxane) and F) RhB (RhB in water). All spectra were recorded at $\lambda_{ex} = 422$ nm, the peaks at 495 nm correspond to the Raman scattering of water. Reprinted from ref. [106] with permission from ACS. (https://pubs.acs.org/doi/10.1021/acs.macromol.5b02152. Further permissions related to the material excerpted have to be directed to ACS.)

fluorophore and the solvent,[107] making such micelles a versatile tool in the fields of biology, medicine, or chemical sensor applications.

However, solvation-responsiveness can also be applied to better understand chemical reaction mechanisms and thus, to develop soft matter smart materials in a more precise and straightforward manner. Until recently, it was challenging to gain further insight into the mechanism of precipitation polymerization, although this reaction is of key interest in industry due to its surfactant-free nature, size control and functionality tolerance. While it was only suggested that the process includes two steps, namely nucleation and the growth,[108,109] Tang and co-workers were able to monitor the different stages of the reaction directly in a self-reporting manner by using fluorophores with aggregation-induced emission (AIE) properties.[108] A 4-vinylbenzyl-modified tetraphenylethylene (TPE–VBC) was synthesized with typical AIE-characteristics, more precisely showing only weak emission in solution, yet strong fluorescence upon aggregation in the precipitated polymers. During the precipitation polymerization with styrene, maleic anhydride and azobisisobutyronitrile (AIBN), the previously transparent solution becomes turbid, the fluorescence intensity strongly increases and can be monitored under daylight or UV light, as demonstrated in Figure 12. Evaluation of the various analytical results (microscopy (TEM, SEM, CLSM), dynamic light scattering (DLS) and UV/Vis/Fluorescence spectroscopy) allows for the detailed characterization of the underlying mechanism and the precise allocation of the different reaction steps. Besides the in situ monitoring of the reaction progress, the obtained polymeric fluorescent particles (PFPs) with uniform ($PDI_{DLS} < 0.15$) and tunable sizes possess bio-labeling and photosensitizing properties for imaging and therapy applications. The authors successfully coated the PFPs onto Natural Killer (NK) cells, which play a crucial role in the immune system as defense against infection and cancer cells. Indeed, the coated PFP-NK cells revealed advanced immu-

notherapy efficiency towards cancer cells in comparison to non-coated NK cells, which can be easily followed by fluorescence analysis. This enhanced efficiency is attributed to the photosensitizing behavior of the TPE–VBC. Irradiation with light induces the generation of reactive oxygen species (ROS), which in turn triggers the immunotherapy activity of the NK cells. While native NK cells and PFP-coated NK cells show similar immunotherapy activity towards cancer cells in the absence of light, a higher immunotherapy activity was obtained for the PFP-coated NK cells under light irradiation (xenon lamp, $1 \, KW \, m^{-2}$).

Thus, similar to the previously introduced pH-responsive materials, such solvation-responsive polymeric self-reporting materials are auspicious for future developments in biomedical and analytical technologies.

2.5. Light-Responsive Materials

The ability to trigger and control chemical reactions by light is a critical method in various fields in chemistry, materials science, and biomedicine. This is attributed to the rather rapid associated process at ambient temperature, spatiotemporal controllability, and enhanced penetration depths at low energies in the visible light range (400–800 nm), which is especially critical for biomolecules to prevent undesired damage.[110–114] By combining photo-sensitive moieties with self-reporting properties, a powerful tool for sensing and in situ monitoring applications is created. For example, Tang and co-workers took advantage of photosensitive aggregation-induced emission fluorogens (AIEgens), namely tetraphenylethenethiophene (TPETP) and tetraphenylsilole (TPS), with different-colored AIE (red for TPETP and green for TPS).[115] Both AIEgens were incorporated into a peptide substrate with a caspase-3/-7 responsive amino acid sequence Asp-Glu-Val-Asp (DEVD) between the two AIEgens and a cyclic amino acid sequence Arg-Gly-Asp (cRGD) at the TPS-containing chain end to enable the cell uptake, as depicted in Figure 13 A.

Upon cell up-take (step 1 in Figure 13 B), TPETP is cleaved from the peptide substrate by intracellular glutathione, and the red emission ($\lambda_{em} = 650$ nm) is turned on (step 2 in Figure 13 B). Subsequent irradiation with light triggers the cleaved TPETP to generate reactive oxygen species (ROS), which in turn induce cell apoptosis and activate the caspase-3/-7 enzyme (step 3 in Figure 13 B). The activated caspase enzyme cleaves the DEVD sequence from the apoptosis sensor and the green fluorescence ($\lambda_{em} = 480$ nm) of the TPS is turned on (step 4 in Figure 13 B). In this way, a self-reporting system for application as photosensitizer (PS) in photodynamic therapy (PT) is created, allowing the real-time monitoring of PS activation and therapeutic response simultaneously by simple color change of the AIE.

Similarly, the in situ monitoring of cell apoptosis was recently reported by applying a new, yet related AIEgen tetraphenylethene–tetraethylpyridinium iodine (TPE-4EP +).[116] This AIEgen proved to have remarkable selectivity for cancer cells accompanied by an efficient
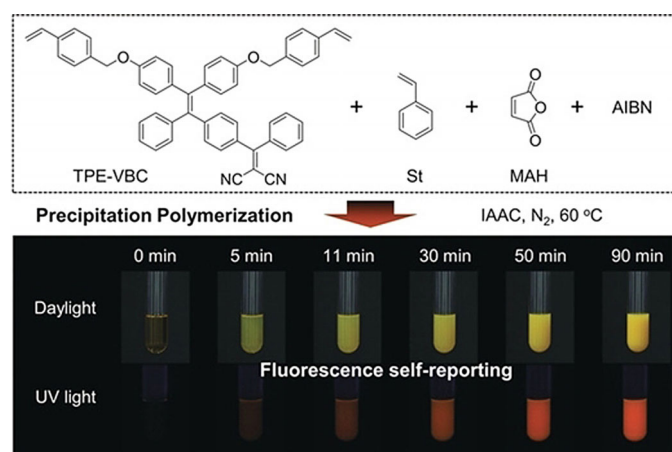

Figure 12. Precipitation polymerization of the AIEgen TPE–VBC with styrene, maleic anhydride, and AIBN in isopentyl acetate (IAAC) at 60 °C under inert atmosphere. The progress of the reaction was monitored under daylight and UV light in specific time intervals. Reprinted from ref. [108]. Copyright 2020 Wiley-VCH GmbH, Weinheim.
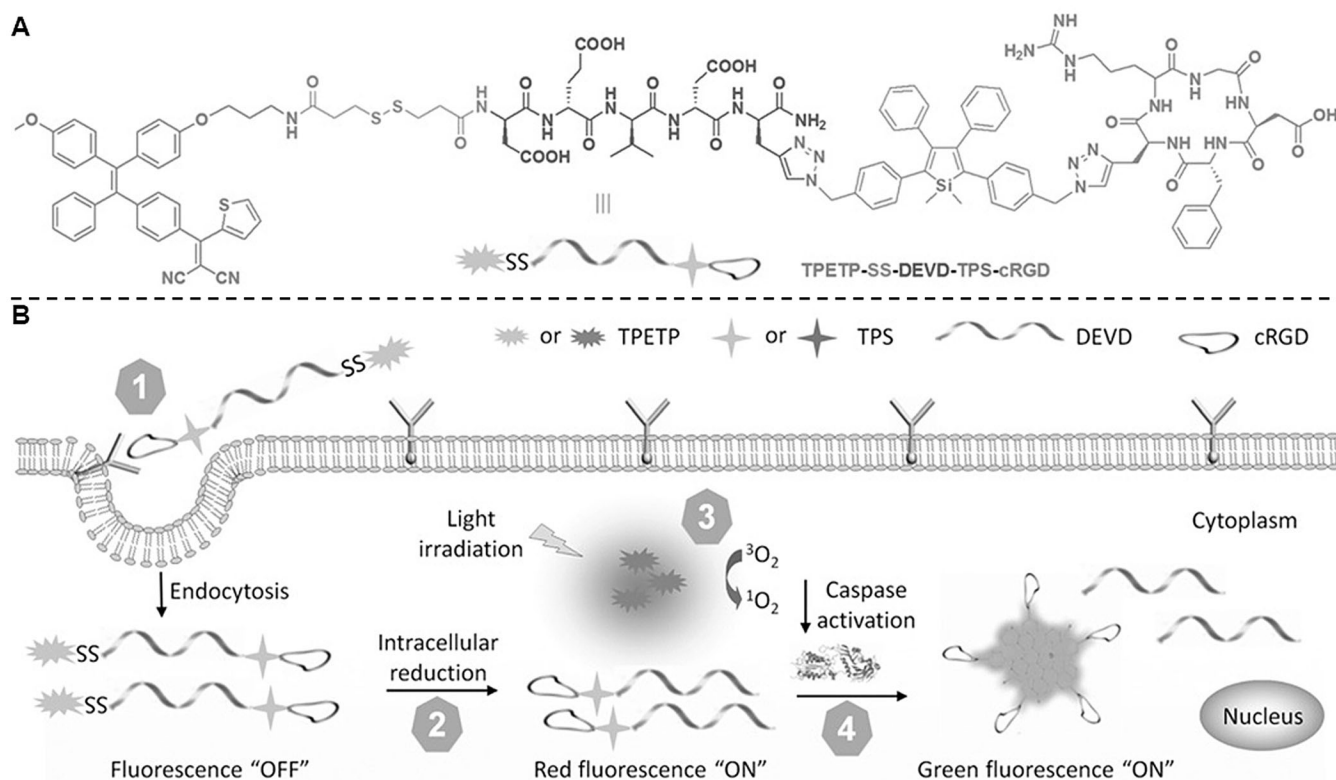
Figure 13. A) Structure of the TPETP- and TPS-containing peptide substrate with a caspase-3/-7 responsive amino acid sequence Asp-Glu-Val-Asp (DEVD) and a cyclic cell uptake enabling amino acid sequence Arg-Gly-Asp (cRGD). B) Process of the self-reporting PS activation and therapeutic response. 1: Cell uptake via the cRGD end group (endocytosis). 2: Intracellular reduction by glutathione cleaves the S—S bond and the TPETP is released, indicated by the red fluorescence. 3: Irradiation with light triggers the TPETP to generate ROS, which in turn activate the caspase enzyme. 4: The activated caspase enzyme cleaves the DEVD sequence from the apoptosis sensor and the green fluorescence of the TPS is turned on. Reprinted from ref. [115]. Copyright 2015 Wiley-VCH GmbH, Weinheim.

ROS (specifically $^1O_2$) generation. The selectivity towards cancer cells is attributed to electrostatic interactions between the negative transmembrane potential of the dysfunctional mitochondria within cancer cells and the positively charged pyridinium moieties in the TPE-4EP+. Upon cell uptake of the AIEgens into the cancer cell, an increased fluorescence emission is measured in contrast to normal cells, which did not take up the AIEgen. Irradiation with white light (4.2 mW cm^{-2}, 400–700 nm) induces the formation of $^1O_2$ and thus, cell apoptosis. Since the apoptosis process leads to a depolarization of the mitochondrial membrane potential and an increased cell permeability, the AIEgen is cleaved form the mitochondria and relocated to the nucleus via electrostatic interactions with the nuclear DNA. Although the introduced studies are merely a proof-of-concept, they surely promise to improve therapeutic treatments and evaluation of therapeutic responses. With future developments on AIEgens that display prolonged absorption and emission wavelengths, the way is paved for multifunctional, self-reporting in vivo applications.

Complementary to the self-reporting output of the precipitation polymerization introduced in Section 2.4 (Figure 12), methods have been developed to monitor the progress and monomer conversion during light-triggered polymerization processes. For example, a porphine zinc derivative applied in a photo-induced electron/energy transfer (PET) RAFT polymerization as photocatalyst enabled the real-time monitoring of the monomer conversion via changes in the fluorescence emission.[117] Another possibility is the application of the nitrile imine-mediated tetrazole–ene cycloaddition (NITEC) reaction, displayed in Scheme 1. Under light irradiation, nitrogen is released from the tetrazole moiety and a nitrile–imine dipole is generated, which subsequently undergoes a 1,3-dipolar cycloaddition with an alkene to yield a highly fluorescent five-membered pyrazoline cycloadduct. By taking a bifunctional tetrazole chain transfer agent (CTA) and a bismaleimide, fluorescent polymers are formed in a step-growth fashion upon irradiation at 320 nm.[118] While the initial reaction mixture shows no fluorescence emission, the poly(pyrazoline)s exhibit a broad fluorescence emission between 470 and 670 nm and thus, the progress of the reaction can be easily followed by fluorescence spectroscopy. Similarly, the NITEC reaction has been applied to monitor the formation of polymeric networks and their characterization.[119] Polymers having tetrazole chain termini can be crosslinked into polymeric networks in the presence of trimaleimides under UV irradiation. For each crosslinking point, one fluorescent pyrazoline ring is formed and the kinetics of the network formation can be monitored in a quantitative way. Therefore, an effective self-reporting

method is presented for the facile and detailed characterization of polymer networks, which so far has been often challenging due to the complexity of the network systems.

Furthermore, light has been used as trigger for the intramolecular collapse of well-defined polymers to yield single-chain nanoparticles (SCNPs). In recent years, the research into SCNPs has gained intensive attention since they find applications in catalysis, drug delivery, protein mimics, or sensing. Among the various synthesis strategies for tailor-made SCNPs, the photo-induced chain collapse displays a mild and versatile pathway, especially when combined with self-reporting properties. Thus, different strategies for the crosslinking have been developed, ranging from the earlier introduced NITEC reaction to single-chain collapse based on radical species. By incorporating nitroxides[120] or pyrene-substituted oxime esters[121] into polymers, light irradiation results in the formation of SCNPs with the ability to self-report the status of the folding. On the one hand, nitroxide-containing polymers exhibit no fluorescence in the unfolded state, whereas folding in the presence of a crosslinker into SCNPs leads to a broad emission between 380 and 550 nm, as can be seen in Figure 14 A. Oxidation with mCPBA reverses the process and the non-fluorescent, unfolded polymer is regained (Figure 14 A). On the other hand, pyrene-substituted oxime ester polymers show the inverse behavior. While the unfolded polymer chain exhibits broad fluorescence emission between 400 and 800 nm due to the incorporated pyrene unit, light irradiation splits the oxime ester and the pyrene unit is cleaved from the polymer. Since also CO_2 can

be released during the reaction, the polymer chains have several possibilities to crosslink, as illustrated in Figure 14 B. Thus, by carefully choosing the incorporated species into polymer backbones, SCNPs with self-reporting characteristics depending on the folding-state are accessible. In this way, powerful tools for prospective biomedical, imaging, or sensor applications can be constructed, however, limitations such as folding in highly diluted media ($c = 20\ \mathrm{mg\,L^{-1}}$) or complex monomer and polymer synthesis need to be overcome for industrial purposes.

2.6. Chemically Responsive Materials

The discussion in the previous section on light-responsive materials revealed the importance of light as trigger for self-reporting properties. However, light is not only able to induce the self-reporting, but may also be the self-reporting characteristic itself. Light as direct output of a chemical reaction, that is, chemiluminescence (CL),[122–125] offers beneficial advantages such as high sensitivity and real-time monitoring over a wide dynamic range without the need for sophisticated equipment.[124,126–130] Therefore, CL reactions find widespread applications in biomedical or analytical fields with ongoing research for persistent improvement. However, the challenge to gain higher CL quantum yields, tune the emission range, or simplify the CL system is to modify the reaction environment or the luminophore itself in such a way that the CL properties are not diminished accidentally. Nevertheless, recent research into common luminophores, such as dioxetanes,[131,132] peroxyoxalates (POs),[122,133–137] acridinium esters,[138–141] luminol,[129,142] and their respective derivatives, led to the development of a plethora of advanced, promising self-reporting CL systems. The CL of acridinium esters, for example, can be triggered by antioxidants, enzymes or peroxides and thus finds application in (biomedical) analytics as self-reporting sensor for these substances.[138–141] In the presence of a trigger, the acridinium esters are oxidized to dioxetanones, which decompose with the release of CO_2 to form the highly emissive 10-methyl-9-acridone,[139,143] as displayed in Scheme 2 A. So far, alkaline conditions were required for the CL emission of acridinium esters. However, recently, acridinium ester derivatives were synthesized which allow the CL reaction to proceed under neutral conditions. This was achieved by introducing electron withdrawing groups (e.g. cyano, nitro, bromide, or trifluoromethyl) in the 4-position of the phenol moiety.[139] Addition of cetyltrimethylammonium bromide also resulted in an increased CL of such acridinium ester derivatives.[140]

Similarly, peroxyoxalate (PO) luminophores are ideally suitable for analytical methods in food and environmental analysis, sensor technology, pharmacology, biology, or medicine.[122,135,136] As for the acridinium esters, the CL reaction of POs can be induced by various active species such as peroxides, microorganisms, glucose, toxins, or antioxidants.[122,144] Oxidation of POs, such as the bis(2,4,6-trichlorophenyl)oxalate (TCPO), results in the decomposition of the PO and the formation of an unstable energy-rich dioxetanone. In contrast to the acridinium esters however, the
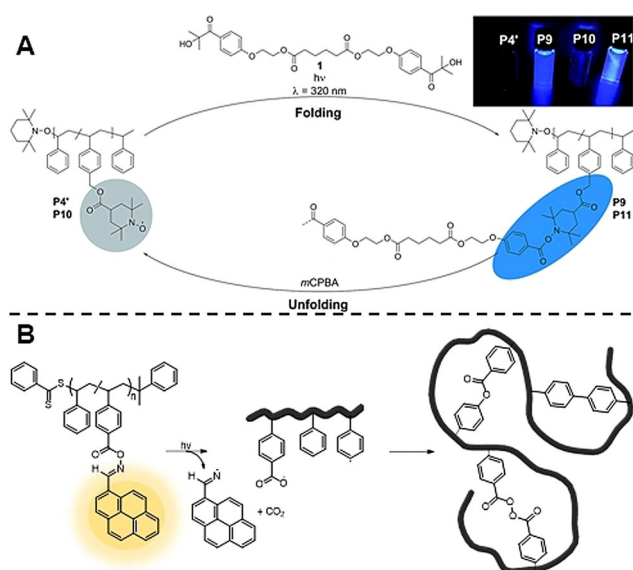

Figure 14. A) Folding process of the nitroxide-containing polymer. In the presence of a crosslinker, the non-fluorescent polymer is folded into a fluorescent SCNP under irradiation with light. Oxidation with mCPA cleaves the crosslinker and the unfolded, non-fluorescent polymer is regained. Reprinted from ref. [120], published by the Royal Society of Chemistry. B) Intramolecular chain collapse of the fluorescent pyrene-substituted oxime ester polymer. Light irradiation splits the oxime ester and the fluorescent pyrene unit is cleaved form the polymer. Subsequently, the polymer chains have several possibilities to crosslink via radical coupling.
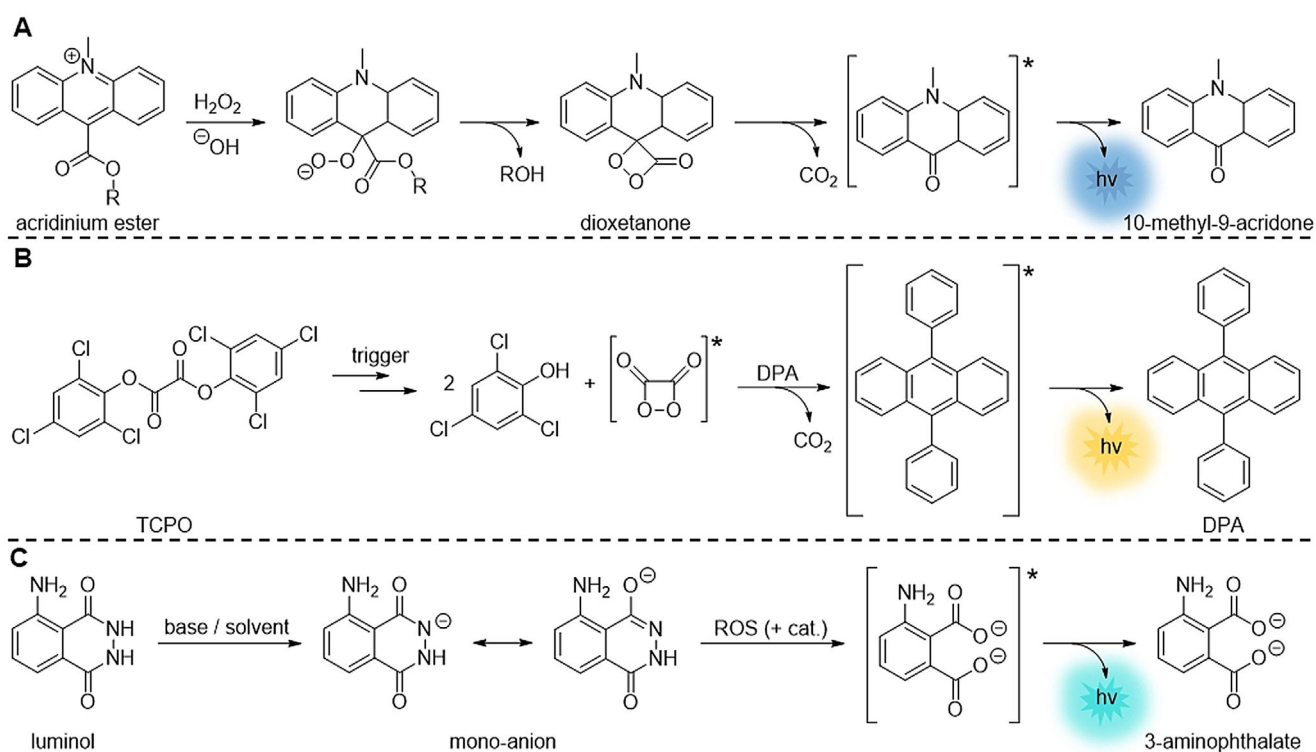
Scheme 2. CL reaction pathways of A) acridinium esters, B) POs in the presence of a fluorophore, and C) luminol.

decomposition of the dioxetanone into CO_2 does not result in the emission of light unless a fluorophore is present. In the presence of the latter, for example, 9,10-diphenylanthracene (DPA), the decomposition of the dioxetanone evokes excitation of the fluorophore and light is emitted during the relaxation into the ground state,[133] as can be seen in Scheme 2B. Although the need for an additional fluorophore for the CL reaction could be seen as disadvantage, the possibility to readily adjust the emission wavelength from the UV/Vis to the NIR spectral range on demand by carefully choosing the fluorophore, rather than modifying the luminophore in a (complicated) synthesis strategy, clearly outweighs the need for two components.[134] Indeed, recently, the successful combination of the PO moiety and the fluorophore in one material was reported to enable solid-phase CL read-out.[133] This was achieved by synthesizing microspheres with a poly(divinylbenzene) core and a poly(2-hydroxyethyl methacrylate) shell, allowing the subsequent functionalization with a tetrazole carboxylic acid. Finally, a maleimide-PO (MDCPO) was photochemically linked to the tetrazole-containing microspheres via the aforementioned NITEC reaction, as presented in Figure 15A. The obtained "all-in-one" microspheres provide high fluorescence and CL emission at low concentration of oxidative species, thus acting as a self-reporting sensor for these oxidative species. In addition, the emission wavelength of the light output can be readily tuned by varying the incorporated tetrazole moieties. With the use of red-shifted tetrazoles, such microspheres are also applicable for biological systems and the solid-phase CL holds key potential to exceed current PO-CL multicomponent

systems for sensing and detecting low concentrations of active species in a self-reporting manner.

Correspondingly, the improvement and simplification of complex CL systems has emerged into the field of the luminol chemistry. The well-known and most adopted luminophore in forensic science[145,146] offers advantages such as low cost, broad analytical compatibility and expansive application spectrum.[147,148] Similar to the CL of PO, the CL of luminol is triggered by an oxidation reaction. As depicted in Scheme 2C, luminol is present in its deprotonated species, namely the luminol mono-anion, in (basic) solution, and addition of an oxidant (e.g. ROS), the mono-anion is oxidized to the excited 3-aminophthalic acid, whose decay to the ground state is accompanied by a striking blue–green light. Unfortunately, the CL quantum yield of luminol is rather low in polar aprotic solvents, such as DMSO, or aqueous media,[123] thus diverse catalytic systems containing nano-materials,[130,149–152] metal ions,[147,148] or other enhancers[153–155] have been developed to improve the CL emission. Since all these systems suffer from individual disadvantages (cost, toxicity, air/moisture sensitivity, or stability issues, amongst others), the development of new, advanced luminol-CL systems is of high importance. The critical point for achieving such improved luminol-CL systems is to identify a way to reduce the number of components to a minimum, while simultaneously boosting CL emission. Indeed, significant improvements were achieved by implementing an organic superbase, namely 1,5,7-triaza-bicyclo-[4.4.0]dec-5-ene (TBD), into the oxidation reaction of luminol.[142] Superbases such as TBD find widespread application in organic synthesis and provide high pK_a values (26.0 in acetonitrile for TBD),
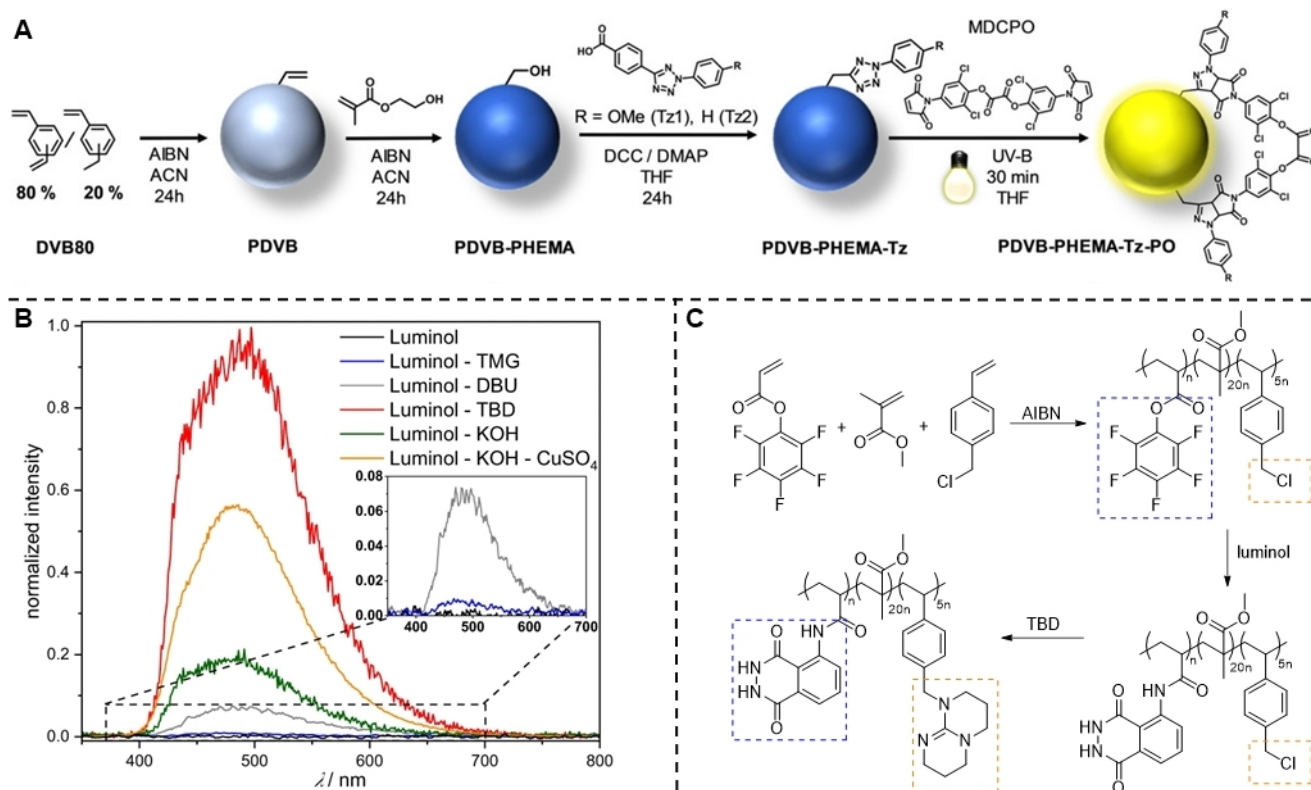
Figure 15. A) Synthesis of polymeric tetrazole- and maleimide-PO-containing microspheres for solid-phase CL read-out. Reprinted from ref. [133]. Copyright 2019 Wiley-VCH GmbH, Weinheim. B) CL emission of luminol-(super-)base systems in DMSO at ambient temperature, triggered by H_2O_2. Reprinted form ref. [142]. Copyright 2019, Springer Nature. C) Synthesis of the luminol–TBD-containing polymer via free radical polymerization and subsequent post-polymerization modification. Reproduced from ref. [129], published by the Royal Society of Chemistry.

combining two essential characteristics—basicity and catalysis—for the CL reaction of luminol in one molecule. Upon addition of H_2O_2 to a solution containing only TBD and luminol, a striking blue light visible even with the naked eye is observed. Comparison of the CL emission of the luminol–TBD system with the organic superbases 1,1,3,3-tetramethylguanidine (TMG) and 1,8-diazabicyclo[5.4.0]undec-7-ene (DBU) as well as with the already known inorganic base KOH and catalyst $CuSO_4$, respectively, revealed the superior CL emission of the luminol–TBD system, which can be clearly seen in Figure 15B. Importantly, in contrast to conventional inorganic bases applied in the luminol-CL reaction, organic superbases offer the possibility to be incorporated into polymeric materials. Without the need for a (complicated) TBD-monomer synthesis, the TBD itself could be readily incorporated into the same polymeric backbone as luminol via a post-polymerization modification (PPM) approach, as demonstrated in Figure 15 C.[129] The post-modified polymer further enables supramolecular (dis)assembly with randomly methylated β-cyclodextrin, analogous to the binding behavior between biomolecules and substrates, which results in a strong CL output that can be detected without the need for sophisticated instrumentation, such as nuclear magnetic resonance (NMR) and dynamic light scattering (DLS). Therefore, the implementation of organic superbases to the CL reaction of luminol on the small molecule as well as on the macromolecular level not only expands the scope of luminol

chemistry, but also paves the way for the design of new, artificial luminol materials in sensor technology or biomedical applications. Chemically responsive materials are of substantial interest in the fields of sensor, diagnostic, or biomedical technology due to their fast and sensitive detection of specific active species via a chemiluminescent output, visible even to the naked eye. Hence, such CL materials will certainly play a crucial role not only in future analytical processes, but also in the fast detection of (new) diseases and (benign/malignant) biomolecules.

2.7. Multi-Stimuli-Responsive Materials

So far, self-reporting systems have been discussed which are responsive to one exclusive stimulus shown in Scheme 1. However, there exist substrates that are able to respond to various stimuli, depending on the substituents of the self-reporting unit and the stimulus.[156–161] One important class providing such multi-responsiveness are light emitting 1,2-dioxetanes. In contrast to the aforementioned CL systems in Section 2.6, the CL of 1,2-dioxetanes can not only be triggered by chemical reactions, but also by mechanical forces and temperature. The thermal decomposition of 1,2-dioxetanes accompanied by the emission of light has already been reported in the 1970s.[162–164] Though elevated temperatures of up to 250 °C[165,166] were required to induce decomposition, the
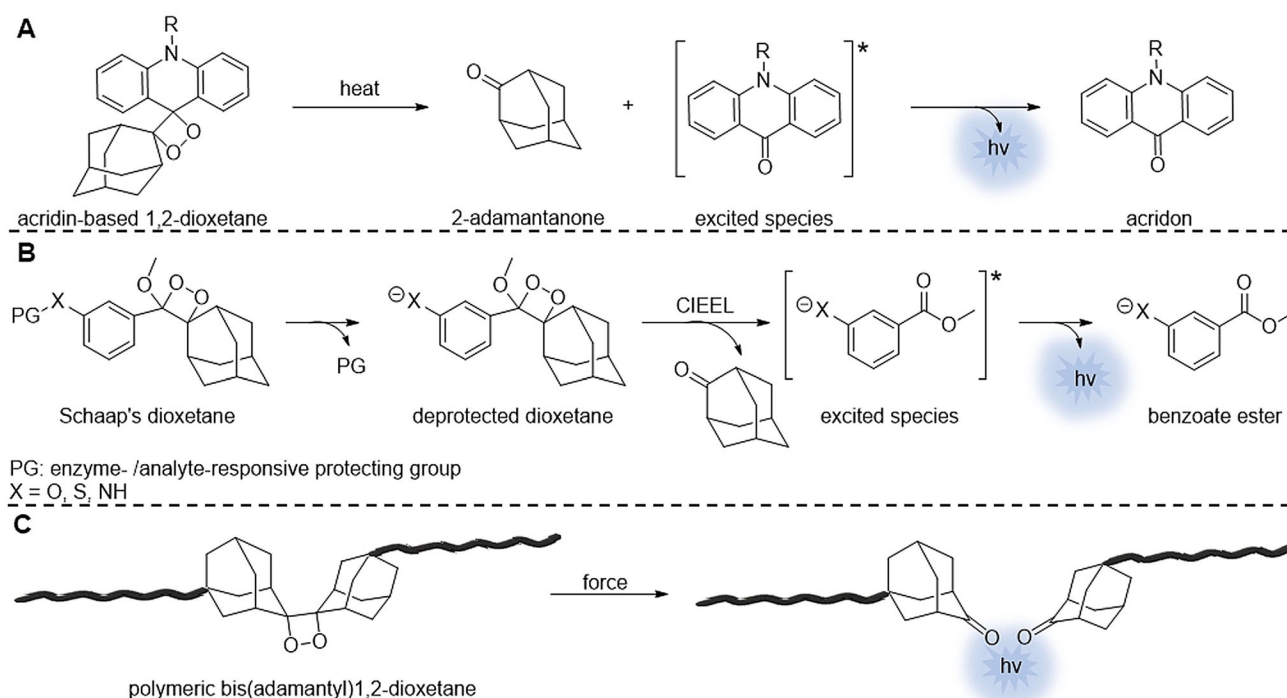
Scheme 3. CL triggering mechanism of A) thermo-responsive, B) chemically responsive, and C) mechano-responsive 1,2-dioxetanes.

research into thermo-responsive 1,2-dioxetane derivatives was disregarded except for a few examples reported by Roda and co-workers.[165–170] By synthesizing acridine-based 1,2-dioxetane derivatives as depicted in Scheme 3 A, temperatures between 80 and 110 °C lead to the decomposition into 2-adamantone and an excited acridone species, which emits light upon returning to the ground state (similar to the 10-methyl-9-acridone of the acridinium ester CL, Scheme 2 A).

On the other hand, significantly more research has been conducted to broaden the responsiveness of 1,2-dioxetanes towards chemical/biological stimuli. Based upon Schaap's findings in 1987,[131,132] a plethora of chemiluminescent 1,2-dioxetane derivatives have been developed. Generally, a 1,2-dioxetane with an enzyme- or analyte-responsive protecting group was synthesized, whose removal triggers the chemically initiated electron-exchange (CIEEL) process. During this process, the deprotected dioxetane decomposes and an excited benzoate ester species is obtained, which returns to the ground state accompanied by the emission of light (Scheme 3 B).[123,125,132] By carefully choosing the phenol substituents (and their position) of Schaap's dioxetane discovered in 1987, a plethora of CL 1,2-dioxetane derivatives for (bio-)labeling and imaging have been developed, which are also suitable for in vivo applications under physiological conditions.[126,171–177]

Besides the thermal and chemical activation, the CL of 1,2-dioxetanes can also be triggered by mechanical forces. The incorporation of bis(adamantyl)1,2-dioxetanes into polymeric materials (e.g. polyurethane,[178–181] poly(methyl methacrylate),[182] poly(methyl acrylate),[183,184]) poly(dimethylsiloxane)[185]) enabled the facile, real-time monitoring of bond breaking events in such materials, since mechanical force leads to a bond scission of the dioxetane moiety into two adamantone-terminated polymer chain visualized by the emission of light, as can be seen in Scheme 3 C. Clearly, 1,2-dioxetanes represent an important class for the development of versatile, smart, self-reporting materials since the CL can be easily tailored to the desired stimulus by thorough choice of the respective 1,2-dioxetane derivative.

Another important class of self-reporting materials are liquid crystals (LCs). LCs find widespread applications in biology and medicine as well as in photovoltaic systems, displays, opto-electronics, or sensors.[186–191] Such diverse applications are attributed to the beneficial properties of LCs combining the order of crystals with the mobility of liquids. Upon exposure to stimuli (e.g. chemical or biological substrates, electrical fields, temperature, or mechanical forces), the initial order and mobility of the LC is disrupted and the optical appearance is adjusted. Abbott and co-workers took advantage of such self-reporting LCs and expanded the concept by introducing self-regulating properties.[192] This was achieved by synthesizing LC films of 4'-pentyl-4-biphenylcarbonitrile (5CB) dispersed with microdroplets containing a red dye for visualization (Figure 16 A,B). Placed in a mini-well with an overlying aqueous phase, the microdroplets are enclosed by strained LCs. In the presence of a thermal stimulus, the LC undergoes a phase transition and the original state of the LC is disturbed, which is visually indicated by the release of the red microdroplet. Since the phase transition of 5CB already takes place at 35 °C, the heat provided by a human finger is able to trigger the phase transition (Figure 16 C–E). Precisely at the moment when the phase transition takes place, a specific amount of microdroplets is released, and subsequently the release stops.
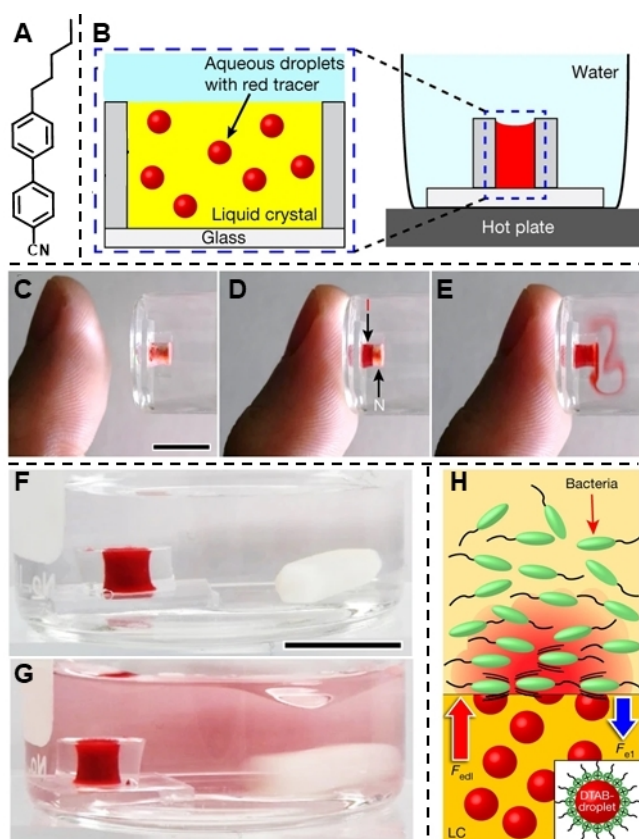
Figure 16. A) Structure of the LC 4′-pentyl-4-biphenylcarbonitrile (5CB). B) Dispersion of microdroplets in 5CB hosted in a mini-well, which is immersed in an overlying aqueous phase. C–E) The heat of a human finger applied to release the microdroplets from the LC. F,G) Release of microdroplets from the LC F) before and G) after inducing mechanical stress by stirring of the overlying aqueous phase. H) Bacteria-induced release of the microdroplets. Reprinted by permission from Springer nature, ref. [192], Copyright 2018.

This behavior can be observed for several heating/cooling cycles, making the system self-regulating. In contrast, conventional materials released their loadings unless the trigger was removed or the loading was completely released.

In addition, the disturbance of the LC can be induced by mechanical forces, as displayed in Figure 16 F,G. While the LC does not release microdroplets into the overlying aqueous phase in the passive state (Figure 16 F), the aqueous phase turns red upon mechanical shear stress induced by magnetic stirring (Figure 16 G). Interestingly, motile bacteria are also able to induce mechanical stress and thus trigger the release of microdroplets (Figure 16 H). If the microdroplets are filled with an additional antibacterial agent (cationic DTAB and silver salts), the release of the droplets not only reports the presence of bacteria in a visible way, but also induces the killing of the bacteria. The dead bacteria are not moving anymore, thus there no longer exists a mechanical force and the release stops. Clearly, the combination of self-reporting and self-regulating properties in LCs responding to several stimuli holds great potential for future developments of programmable materials. Various systems with the desired stimuli-responsive properties can be designed by carefully choosing the LC material and the composition of the micro-droplets.

Correspondingly, the isomerization of the previously introduced spiropyrans (SP, see Section 2.1) into merocyanine (MC) can not only be induced by mechanical forces, but also by, for example, temperature, pH, solvation, or light.[193–200] Intriguingly, SP-based self-reporting systems have been developed that respond to several stimuli simultaneously.[46–47,201–204] For example, Qui et al. reported the synthesis of poly(hydroxyethyl acrylate) with incorporated SPs, which changed color upon light irradiation or swelling in water.[205] Furthermore, amphiphilic copolymers have been synthesized bearing SP moieties that self-assembled into micellar nanoparticles triggered by either light, pH, or temperature.[206] In another example, Mondal et al. synthesized an organic cage functionalized with SP units, which change their color from yellow to orange in the presence of thermal or photochemical stimuli.[207] This behavior was observed in solution and in the solid state. Tests of up to 20 UV/Vis- and heating/cooling cycles in both states proved the reversibility of the SP–MC isomerization upon thermal or photochemical treatment.

Similarly, luminogens such as hexakis(pyridine-4-ylthio)-benzene show different-colored phosphorescence in the liquid and solid state depending on the applied stimulus (e.g. solvent, pH, metal ions).[208] Additionally, networks with a coordinated triphenylamine fluorophore have been synthesized which gradually change their emission color depending on either temperature (from cyan to green) or pressure (green to red) in a reversible manner.[209]

Such self-reporting multi-stimuli-responsive properties hold key potential for the development of innovative smart materials which are exposed to several stimuli at the same time, for example, outdoor materials or materials operational in extreme environments. Materials often need to defy different stimuli simultaneously, for example, temperature and light (winter/summer, heating/air conditioning, natural/artificial light, day/night,), chemicals (pollution, cleaning agents, aerosols), mechanical forces (wind, earth quakes, thunder), and weather conditions (rainy, dry, humid, foggy). Therefore, the ability to report any damages or changes evoked by an interaction of several stimuli in a visible manner would help to increase the lifetime and safety of the materials. Additionally, costs could be reduced due to a prolonged lifetime and more effective maintenance.

3. Self-Reporting Materials as (Biomedical) Diagnostic Tools

Throughout the current Review, we already indicated the significance of self-reporting materials in the field of biology, medicine, and analytics. Since the importance of novel, innovative materials in these fields has become particularly evident in consideration of the current SARS-CoV-2 (COVID-19) pandemic,[210–213] the current chapter focuses on self-reporting materials as (biomedical) diagnostic tools. For instance, the detection of important biological substrates (e.g. biothiols) that influence physiological processes often requires sophisticated and complex analytical methods such

as HPLC, capillary electrophoresis separations, and immuno-assays, and time-consuming sample preparations are required.[214–216] Therefore, self-reporting systems based on fluorescence changes have been developed for the simple and fast detection of biothiols. These biothiols include cysteine (cys), homocysteine (hcy), glutathione (GSH), or hydrogen sulfide (H_2S), which are responsible for cell mobility and degradation, maintaining redox homeostasis and xenobiotic metabolism, apoptosis, or anti-inflammation. In addition, deviations from regular levels serve as indicators for disorders (Alzheimer, cardiovascular diseases, slowed growth, liver damage, or lethargy, amongst others).[217–219] While several systems have been developed for the selective detection of single cys,[220–223] cys/hcy,[214] or GSH,[214,215] the production and metabolism of the biothiols are interconnected and often two or more of the biothiols are present at the same time. Therefore, it would be highly beneficial to have sensor molecules for the simultaneous detection of such bio-thiols.[224–226] Despite the similar chemical structure and reactivity, self-reporting materials have been developed that are not only able to detect multiple biothiols, but also to distinguish between them. For example, a coumarin-based fluorescent probe was successfully applied to distinguish between GSH and cys/hcy based on different fluorescent emission behavior.[227] The fluorescence emission can also be altered by taking advantage of the unique binding behavior of the biothiols. Fluorophores with several functional groups, each specifically reacting with a single biothiol, reveal different fluorescence emissions depending on the biothiol and the reacted functionality.[228,229] In another example, a lysosome-targetable probe with both 7-dimethylaminocoumarin and resorufin as fluorophores was synthesized as depicted in Figure 17.[230] The free resorufin exhibits red emission, while the bonded resorufin shows no emission and quenches the fluorescence of the coumarin fluorophore. In the presence of H_2S, cys/hcy, or GSH, the resorufin is cleaved and the red emission is turned on. Depending on the present biothiol, the coumarin fluorophore exhibits different fluorescence emission: no fluorescent product is obtained in the presence of H_2S, whereas a green-emitting product is obtained when GSH is present and a blue-emitting species in the presence of cys/hcy (Figure 17). Thus, the distinctive fluorescence pattern
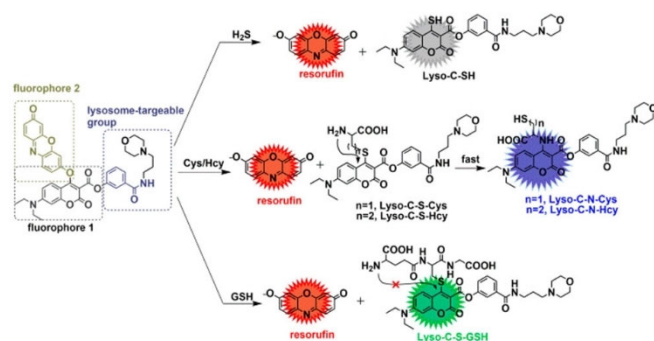
(red, red–green, or red–blue) self-reports the presence of a specific biothiol.

Besides biothiols, pathogens such as bacteria, fungi, parasites, or viruses play a critical role in biology and medicine. Pathogens are responsible for various health issues and diseases (inflammations, (food/water) poisoning, influenza, Middle-East Respiratory Syndrome (MERS) CoV, SARS-CoV-1/-2, cancer).[211,217,218,231–234] Therefore, it would be highly beneficial to detect pathogens in a self-reporting, fast, and efficient manner to stop them from spreading. Indeed, various methods for the self-reporting detection of pathogens have been developed.[235–239] For example, certain pathogens are responsible for elevated levels of enzymes, which can be easily detected in the presence of suitable fluorophores.[231,234,240–242]

Another strategy applies optical sensors with porous Si photonic crystals. The pore size can be adjusted to capture targeted bacteria, for example, *Escherichia coli* (*E. coli*), which results in a reflectivity change. This method allows the facile and sensitive detection of various pathogens due to the tunable size of the pores.[243] Similarly, indium tin oxide screen-printed electrodes were coated with polyaniline (PANI) and antibodies able to capture targeted pathogens (Figure 18).[244] In the absence of pathogens, a constant potential leads to a change in the oxidation state and thus, the color changes from yellow to blue. In the presence of pathogens however, the resistance on the electrode surface is affected and different-colored PANI oxidation states are obtained, depending on the concentration of the pathogen (Figure 18). By carefully choosing the polymeric material and antibody for the electrode coating, various pathogens may be detected in a simple, fast and visible manner.

Clearly, the introduced self-reporting systems for the detection of biological substrates and pathogens hold great potential for innovative, smart materials. Developments towards innovative systems that self-report the presence of any biomolecules or pathogens in a selective and fast way might help to prevent future pandemic outbreaks of diseases. First of all, the presence of a new potential pathogen (such as the current pandemic virus) needs to be detected before it can spread worldwide. On the other hand, rapid analytical results

Figure 17. Various fluorescence emission patterns of the lysosome-targetable probe in the presence of H_2S, cys/hcy, and GSH. Reprinted from ref. [230], Copyright 2018 American Chemical Society.
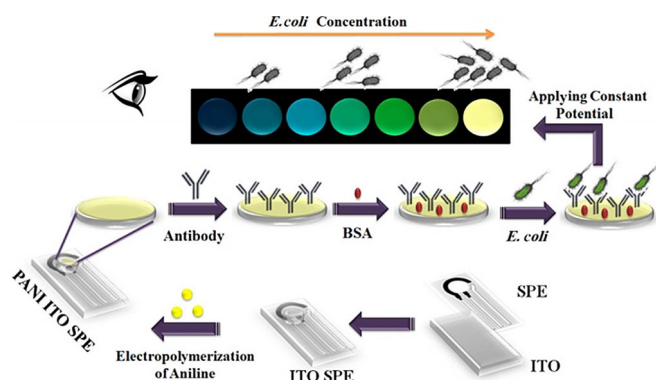

Figure 18. Coated electrodes with polyaniline and antibodies for the visual detection of pathogens. Reprinted from ref. [244], Copyright 2019 American Chemical Society.

will disburden clinical laboratories and infected patients could be isolated immediately to reduce the risk of infection.

Inspiring ideas such as virucidal-active personal protective equipment,[212] antiviral surface coatings,[212] or even self-sanitizing surfaces[210] have been suggested. Since pathogens are not only transmitted via surfaces but, more importantly, via the air, future aerosols with self-reporting properties and possible antiviral activities would surely prove as a powerful tool to combat and contain pathogens.

4. Summary and Outlook

The significant growth of studies on stimuli-responsive materials within the past decade indicates the importance and demand for further research and developments of such materials. While stimuli-responsive materials with self-healing properties remain mainly laboratory proof-of-concept constructs, stimuli-responsive materials equipped with self-reporting properties already find application in the industry. Examples are thermo-responsive inks, forensic chemiluminescent mixtures, or liquid crystal displays. However, there are still key challenges that need to be overcome to broaden the possibilities for commercial application: (i) the design of self-reporting materials is hampered by multi-step synthesis, low yield, high-cost, and non-practical up-scaling; (ii) the self-reporting function is often limited in terms of reactive functions, cycles or mobility; (iii) high energy input is required for self-reporting, particularly in the presence of heat or UV light as stimuli, which tend to be replaced by softer stimuli, such as visible light; and (iv) self-reporting is generally limited to detecting nano- or microscopic damages. Therefore, the development of self-reporting materials addressing these issues is of high relevance to the field. Indeed, future progress will likely be driven by the combination of the different concepts described in the present Review. Importantly, the combination of chemical or physical feedback mechanisms within a single material appears to be an attractive option to ensure that a material change is indeed reported. Finally, the development of combinatorial spectroscopic techniques in conjunction with detailed knowledge regarding the self-reporting mechanisms still remains in its early stages, yet is a key factor for designing efficient systems.

Acknowledgements

Conflict of interest

The authors declare no conflict of interest.

[1] S. Wang, M. W. Urban, *Nat. Rev. Mater.* **2020**, *5*, 562.
[2] J. A. McCune, S. Mommer, C. C. Parkins, O. A. Scherman, *Adv. Mater.* **2020**, *32*, 1906890.
[3] J. F. Patrick, M. J. Robb, N. R. Sottos, J. S. Moore, S. R. White, *Nature* **2016**, *540*, 363.
[4] C. E. Diesendruck, N. R. Sottos, J. S. Moore, S. R. White, *Angew. Chem. Int. Ed.* **2015**, *54*, 10428; *Angew. Chem.* **2015**, *127*, 10572.
[5] K. M. Wiggins, J. N. Brantley, C. W. Bielawski, *Chem. Soc. Rev.* **2013**, *42*, 7130.
[6] A. L. Black, J. M. Lenhardt, S. L. Craig, *J. Mater. Chem.* **2011**, *21*, 1655.
[7] M. A. C. Stuart, W. T. S. Huck, J. Genzer, M. Müller, C. Ober, M. Stamm, G. B. Sukhorukov, I. Szleifer, V. V. Tsukruk, M. Urban, F. Winnik, S. Zauscher, I. Luzinov, S. Minko, *Nat. Mater.* **2010**, *9*, 101.
[8] M. M. Caruso, D. A. Davis, Q. Shen, S. A. Odom, N. R. Sottos, S. R. White, J. S. Moore, *Chem. Rev.* **2009**, *109*, 5755.
[9] P. Theato, B. S. Sumerlin, R. K. O'Reilly, I. I. I. T. H. Epps, *Chem. Soc. Rev.* **2013**, *42*, 7055.
[10] O. Speck, T. Speck, *Biomimetics* **2019**, *4*, 26.
[11] Y. Yang, D. Davydovich, C. C. Hornat, X. Liu, M. W. Urban, *Chem* **2018**, *4*, 1928.
[12] Z. Deng, H. Wang, P. X. Ma, B. Guo, *Nanoscale* **2020**, *12*, 1224.
[13] G. Ge, Y. Lu, X. Qu, W. Zhao, Y. Ren, W. Wang, Q. Wang, W. Huang, X. Dong, *ACS Nano* **2020**, *14*, 218.
[14] J. Chen, Y. Huang, X. Ma, Y. Lei, *Adv. Compos. Hybrid. Mater.* **2018**, *1*, 94.
[15] K. Mphahlele, S. S. Ray, A. Kolesnikov, *Polymers* **2017**, *9*, 535.
[16] E. Shchukina, D. G. Shchukin, *Langmuir* **2019**, *35*, 8603.
[17] F. Zhang, P. Ju, M. Pan, D. Zhang, Y. Huang, G. Li, X. Li, *Corros. Sci.* **2018**, *144*, 74.
[18] H. Wang, P. Wang, Y. Feng, J. Liu, J. Wang, M. Hu, J. Wei, Y. Huang, *ChemElectroChem* **2019**, *6*, 1605.
[19] D. Döhler, P. Michael, W. H. Binder, *Acc. Chem. Res.* **2017**, *50*, 2610.
[20] X. K. D. Hillewaere, F. E. Du Prez, *Prog. Polym. Sci.* **2015**, *49–50*, 121.
[21] Q. Zhang, S. Niu, L. Wang, J. Lopez, S. Chen, Y. Cai, R. Du, Y. Liu, J.-C. Lai, L. Liu, C.-H. Li, X. Yan, C. Liu, J. B.-H. Tok, X. Jia, Z. Bao, *Adv. Mater.* **2018**, *30*, 1801435.
[22] R. Hoogenboom, *Angew. Chem. Int. Ed.* **2012**, *51*, 11942; *Angew. Chem.* **2012**, *124*, 12108.
[23] O. Rifaie-Graham, E. A. Apebende, L. K. Bast, N. Bruns, *Adv. Mater.* **2018**, *30*, 1705483.
[24] C. Calvino, C. Weder, *Small* **2018**, *14*, 1802489.
[25] C. P. Kabb, C. S. O'Bryan, C. D. Morley, T. E. Angelini, B. S. Sumerlin, *Chem. Sci.* **2019**, *10*, 7702.
[26] J. Chen, Q. Peng, X. Peng, L. Han, X. Wang, J. Wang, H. Zeng, *ACS Appl. Polym. Mater.* **2020**, *2*, 1092.
[27] Z. Yang, Z. Chi, Z. Mao, Y. Zhang, S. Liu, J. Zhao, M. P. Aldred, Z. Chi, *Mater. Chem. Front.* **2018**, *2*, 861.
[28] E. Inci, G. Topcu, T. Guner, M. Demirkurt, M. M. Demir, *J. Mater. Chem. C* **2020**, *8*, 12036–12053.
[29] J. Geng, W. Li, L. P. Smaga, N. R. Sottos, J. Chan, *Chem. Mater.* **2018**, *30*, 2198.
[30] M. J. Robb, W. Li, R. C. R. Gergely, C. C. Matthews, S. R. White, N. R. Sottos, J. S. Moore, *ACS Cent. Sci.* **2016**, *2*, 598.
[31] S. Chen, T. Han, Y. Zhao, W. Luo, Z. Zhang, H. Su, B. Z. Tang, J. Yang, *ACS Appl. Mater. Interfaces* **2020**, *12*, 4870.
[32] Y. K. Song, T. H. Lee, K. C. Lee, M. H. Choi, J. C. Kim, S.-H. Lee, S. M. Noh, Y. I. Park, *Appl. Surf. Sci.* **2020**, *511*, 145556.

[33] Y. Li, Q. Wang, X. Zheng, Y. Li, J. Luan, *RSC Adv.* **2020**, *10*, 1226.

[34] M. Hu, S. Peil, Y. Xing, D. Döhler, L. Caire da Silva, W. H. Binder, M. Kappl, M. B. Bannwarth, *Mater. Horiz.* **2018**, *5*, 51.

[35] M. Li, Q. Zhang, Y.-N. Zhou, S. Zhu, *Prog. Polym. Sci.* **2018**, *79*, 26.

[36] R. W. Barber, M. E. McFadden, X. Hu, M. J. Robb, *Synlett* **2019**, *30*, 1725.

[37] S. Shree, M. Dowds, A. Kuntze, Y. K. Mishra, A. Staubitz, R. Adelung, *Mater. Horiz.* **2020**, *7*, 598.

[38] A. D. Das, G. Mannoni, A. E. Früh, D. Orsi, R. Pinalli, E. Dalcanale, *ACS Appl. Polym. Mater.* **2019**, *1*, 2990.

[39] X. Zheng, Q. Wang, Y. Li, J. Luan, N. Wang, *Adv. Mater. Technol.* **2020**, *5*, 1900832.

[40] C. Liu, Z. Jin, L. Cheng, H. Zhao, L. Wang, *Nanoscale* **2020**, *12*, 3194.

[41] M. Amjadi, M. Sitti, *Adv. Sci.* **2018**, *5*, 1800239.

[42] Y. Vidavsky, S. J. Yang, B. A. Abel, I. Agami, C. E. Diesendruck, G. W. Coates, M. N. Silberstein, *J. Am. Chem. Soc.* **2019**, *141*, 10060.

[43] Y. Jia, S. Wang, W.-J. Wang, B.-G. Li, S. Zhu, *Macromolecules* **2019**, *52*, 7920.

[44] M. C. Walkey, C. R. Peiris, S. Ciampi, A. C. Aragonès, R. B. Domínguez-Espíndola, D. Jago, T. Pulbrook, B. W. Skelton, A. N. Sobolev, I. Díez Pérez, M. J. Piggott, G. A. Koutsantonis, N. Darwish, *ACS Appl. Mater. Interfaces* **2019**, *11*, 36886.

[45] T. A. Kim, M. J. Robb, J. S. Moore, S. R. White, N. R. Sottos, *Macromolecules* **2018**, *51*, 9177.

[46] S. Shree, M. Schulz-Senft, N. H. Alsleben, Y. K. Mishra, A. Staubitz, R. Adelung, *ACS Appl. Mater. Interfaces* **2017**, *9*, 38000.

[47] S. Rouhani, M. Pishvaei, *J. Fluoresc.* **2017**, *27*, 501.

[48] Y. Sagara, M. Karman, E. Verde-Sesto, K. Matsuo, Y. Kim, N. Tamaoki, C. Weder, *J. Am. Chem. Soc.* **2018**, *140*, 1584.

[49] E. I. Akpan, X. Shen, B. Wetzel, K. Friedrich, in *Polymer Composites with Functionalized Nanoparticles* (Eds.: K. Pielichowski, T. M. Majka), Elsevier, Amsterdam, **2019**, pp. 47.

[50] H. Zhang, X. Zhang, C. Bao, X. Li, F. Duan, K. Friedrich, J. Yang, *Chem. Mater.* **2019**, *31*, 2611.

[51] J.-P. Wang, J.-K. Wang, Q. Zhou, Z. Li, Y. Han, Y. Song, S. Yang, X. Song, T. Qi, H. Möhwald, D. Shchukin, G. L. Li, *Macromol. Mater. Eng.* **2018**, *303*, 1700616.

[52] J.-P. Wang, X. Song, J.-K. Wang, X. Cui, Q. Zhou, T. Qi, G. L. Li, *Adv. Mater. Interfaces* **2019**, *6*, 1900055.

[53] T. H. Lee, Y. K. Song, S. H. Park, Y. I. Park, S. M. Noh, J. C. Kim, *Appl. Surf. Sci.* **2018**, *434*, 1327.

[54] N. Dararatana, F. Seidi, D. Crespy, *Polymer* **2020**, *194*, 122346.

[55] T. Revell, "Genoa bridge collapse—what went wrong and are other bridges at risk?", can be found under https://www.newscientist.com/article/2176962-genoa-bridge-collapse-what-went-wrong-and-are-other-bridges-at-risk/, **2018**.

[56] G. Pianigiani;, E. Povoledo;, R. Pérez-Pena, "Italy Bridge Collapse Leaves 37 Dead", can be found under https://www.nytimes.com/2018/08/14/world/europe/italy-genoa-bridge-collapse.html, **2018**.

[57] David Molloy, Laurence Peter, E. Palmer, "As it happened: Genoa motorway bridge disaster", can be found under https://www.bbc.com/news/live/world-europe-45182675, **2018**.

[58] M. Sponchioni, U. Capasso Palmiero, D. Moscatelli, *Mater. Sci. Eng. C* **2019**, *102*, 589.

[59] Y.-J. Kim, Y. T. Matsunaga, *J. Mater. Chem. B* **2017**, *5*, 4307.

[60] E. M. Frazar, R. A. Shah, T. D. Dziubla, J. Z. Hilt, *J. Appl. Polym. Sci.* **2020**, *137*, 48770.

[61] A. Seeboth, D. Lötzsch, R. Ruhmann, O. Muehling, *Chem. Rev.* **2014**, *114*, 3037.

[62] D. Roy, W. L. A. Brooks, B. S. Sumerlin, *Chem. Soc. Rev.* **2013**, *42*, 7214.

[63] A. J. J. Kragt, N. C. M. Zuurbier, D. J. Broer, A. P. H. J. Schenning, *ACS Appl. Mater. Interfaces* **2019**, *11*, 28172.

[64] C. Zhang, H. Deng, S. M. Kenderes, J.-W. Su, A. G. Whittington, J. Lin, *ACS Appl. Mater. Interfaces* **2019**, *11*, 5393.

[65] H. Y. Lee, Y. Cai, S. Velioglu, C. Mu, C. J. Chang, Y. L. Chen, Y. Song, J. W. Chew, X. M. Hu, *Chem. Mater.* **2017**, *29*, 6947.

[66] W. Zhang, S. Kragt, A. P. H. J. Schenning, L. T. de Haan, G. Zhou, *ACS Omega* **2017**, *2*, 3475.

[67] Y. Liu, Y. Guo, Z. Zhang, Z. Huang, P. Qi, J. Cui, A. Song, J. Hao, *Chem. Commun.* **2020**, *56*, 5315.

[68] Y. Zhou, Y. Cai, X. Hu, Y. Long, *J. Mater. Chem. A* **2014**, *2*, 13550.

[69] H.-N. Kim, S. Yang, *Adv. Funct. Mater.* **2020**, *30*, 1902597.

[70] H. Zhao, Q. Sun, J. Zhou, X. Deng, J. Cui, *Adv. Mater.* **2020**, *32*, 2000870.

[71] J. M. Calm, *Int. J. Refrigeration* **2002**, *25*, 293.

[72] C. Kian Jon, M. R. Islam, N. Kim Choon, M. W. Shahzad, in *Advances in Air Conditioning Technologies: Improving Energy Efficiency*, Springer Singapore, Singapore, **2021**, pp. 1.

[73] M. J. Mendell, Q. Lei-Gomez, A. G. Mirer, O. Seppänen, G. Brunner, *Indoor Air* **2008**, *18*, 301.

[74] O. A. Seppänen, W. J. Fisk, *Indoor Air* **2004**, *14*, 102.

[75] D. Ghosh Dastidar, G. Chakrabarti, in *Applications of Targeted Nano Drugs and Delivery Systems* (Eds.: S. S. Mohapatra, S. Ranjan, N. Dasgupta, R. K. Mishra, S. Thomas), Elsevier, Amsterdam, **2019**, pp. 133.

[76] A. Gandhi, A. Paul, S. O. Sen, K. K. Sen, *Asian J. Pharm. Sci.* **2015**, *10*, 99.

[77] M. Cao, Y. Wang, X. Hu, H. Gong, R. Li, H. Cox, J. Zhang, T. A. Waigh, H. Xu, J. R. Lu, *Biomacromolecules* **2019**, *20*, 3601.

[78] F. Rizzo, N. S. Kehr, *Adv. Healthcare Mater.* **2020**, 2001341.

[79] S. Xian, M. J. Webber, *J. Mater. Chem. B* **2020**, *8*, 9197.

[80] B. Zhang, Y. Cheng, H. Wang, B. Ye, L. Shang, Y. Zhao, Z. Gu, *Nanoscale* **2015**, *7*, 10590.

[81] A. del Prado, D. K. Hohl, S. Balog, L. M. de Espinosa, C. Weder, *ACS Appl. Polym. Mater.* **2019**, *1*, 1399.

[82] A. Beharaj, E. Z. McCaslin, W. A. Blessing, M. W. Grinstaff, *Nat. Commun.* **2019**, *10*, 5478.

[83] A.-C. Ferahian, D. K. Hohl, C. Weder, L. Montero de Espinosa, *Macromol. Mater. Eng.* **2019**, *304*, 1900161.

[84] J. Brandt, J. Lenz, K. Pahnke, F. G. Schmidt, C. Barner-Kowollik, A. Lederer, *Polym. Chem.* **2017**, *8*, 6598.

[85] J. Kötteritzsch, R. Geitner, J. Ahner, M. Abend, S. Zechel, J. Vitz, S. Hoeppener, B. Dietzek, M. Schmitt, J. Popp, U. S. Schubert, M. D. Hager, *J. Appl. Polym. Sci.* **2018**, *135*, 45916.

[86] K. Pahnke, N. L. Haworth, J. Brandt, U. Paulmann, C. Richter, F. G. Schmidt, A. Lederer, M. L. Coote, C. Barner-Kowollik, *Polym. Chem.* **2016**, *7*, 3244.

[87] H. Mutlu, C. W. Schmitt, N. Wedler-Jasinski, H. Woehlk, K. E. Fairfull-Smith, J. P. Blinco, C. Barner-Kowollik, *Polym. Chem.* **2017**, *8*, 6199.

[88] A. M. Schenzel, C. Klein, K. Rist, N. Moszner, C. Barner-Kowollik, *Adv. Sci.* **2016**, *3*, 1500361.

[89] A. M. Schenzel, N. Moszner, C. Barner-Kowollik, *Polym. Chem.* **2017**, *8*, 414.

[90] G. Kocak, C. Tuncer, V. Bütün, *Polym. Chem.* **2017**, *8*, 144.

[91] E. Ratemi, in *Stimuli Responsive Polymeric Nanocarriers for Drug Delivery Applications, Vol. 1* (Eds.: A. S. H. Makhlouf, N. Y. Abu-Thabit), Woodhead Publishing, **2018**, pp. 121.

[92] N. Deirram, C. Zhang, S. S. Kermaniyan, A. P. R. Johnston, G. K. Such, *Macromol. Rapid Commun.* **2019**, *40*, 1800917.

[93] W. Tao, J. Wang, W. J. Parak, O. C. Farokhzad, J. Shi, *ACS Nano* **2019**, *13*, 4876.

[94] J. C. Berkmann, A. X. Herrera Martin, A. Ellinghaus, C. Schlundt, H. Schell, E. Lippens, G. N. Duda, S. Tsitsilonis, K. Schmidt-Bleek, *Int. J. Mol. Sci.* **2020**, *21*, 2513.

[95] Y. Li, L. An, J. Lin, Q. Tian, S. Yang, *Int. J. Nanomed.* **2019**, *14*, 5729.

[96] H. Tang, W. Zhao, J. Yu, Y. Li, C. Zhao, *Molecules* **2018**, *24*, 4.

[97] Z.-Y. Qiao, C.-Y. Hou, W.-J. Zhao, D. Zhang, P.-P. Yang, L. Wang, H. Wang, *Chem. Commun.* **2015**, *51*, 12609.

[98] S. Basak, *Biotechnol. Bioprocess Eng.* **2020**, *25*, 655.

[99] J.-T. Hou, W. X. Ren, K. Li, J. Seo, A. Sharma, X.-Q. Yu, J. S. Kim, *Chem. Soc. Rev.* **2017**, *46*, 2076.

[100] K. Zhang, Y.-J. Gao, P.-P. Yang, G.-B. Qi, J.-P. Zhang, L. Wang, H. Wang, *Adv. Healthcare Mater.* **2018**, *7*, 1800344.

[101] P. Wei, G. Gangapurwala, D. Pretzel, M. N. Leiske, L. Wang, S. Hoeppener, S. Schubert, J. C. Brendel, U. S. Schubert, *Biomacromolecules* **2019**, *20*, 130.

[102] X. Qin, Y. Li, *ChemBioChem* **2020**, *21*, 1236.

[103] A. B. Mabire, Q. Brouard, A. Pitto-Barry, R. J. Williams, H. Willcock, N. Kirby, E. Chapman, R. K. O'Reilly, *Polym. Chem.* **2016**, *7*, 5943.

[104] M. P. Robin, A. B. Mabire, J. C. Damborsky, E. S. Thom, U. H. Winzer-Serhan, J. E. Raymond, R. K. O'Reilly, *J. Am. Chem. Soc.* **2013**, *135*, 9518.

[105] A. Noel, Y. P. Borguet, K. L. Wooley, *ACS Macro Lett.* **2015**, *4*, 645.

[106] M. P. Robin, S. A. M. Osborne, Z. Pikramenou, J. E. Raymond, R. K. O'Reilly, *Macromolecules* **2016**, *49*, 653.

[107] Y. Xie, J. T. Husband, M. Torrent-Sucarrat, H. Yang, W. Liu, R. K. O'Reilly, *Chem. Commun.* **2018**, *54*, 3339.

[108] G. Wang, L. Zhou, P. Zhang, E. Zhao, L. Zhou, D. Chen, J. Sun, X. Gu, W. Yang, B. Z. Tang, *Angew. Chem. Int. Ed.* **2020**, *59*, 10122; *Angew. Chem.* **2020**, *132*, 10208.

[109] Z. Liu, D. Chen, J. Zhang, H. Liao, Y. Chen, Y. Sun, J. Deng, W. Yang, *Research* **2018**, *2018*, 9370490.

[110] F. Politano, G. Oksdath-Mansilla, *Org. Process Res. Dev.* **2018**, *22*, 1045.

[111] D. Cambié, F. Zhao, V. Hessel, M. G. Debije, T. Noël, *Angew. Chem. Int. Ed.* **2017**, *56*, 1050; *Angew. Chem.* **2017**, *129*, 1070.

[112] Q.-Q. Zhou, Y.-Q. Zou, L.-Q. Lu, W.-J. Xiao, *Angew. Chem. Int. Ed.* **2019**, *58*, 1586; *Angew. Chem.* **2019**, *131*, 1600.

[113] N. Corrigan, C. Boyer, *ACS Macro Lett.* **2019**, *8*, 812.

[114] M. Eing, B. T. Tuten, J. P. Blinco, C. Barner-Kowollik, *Chem. Eur. J.* **2018**, *24*, 12246.

[115] Y. Yuan, C.-J. Zhang, R. T. K. Kwok, S. Xu, R. Zhang, J. Wu, B. Z. Tang, B. Liu, *Adv. Funct. Mater.* **2015**, *25*, 6586.

[116] T. Zhang, Y. Li, Z. Zheng, R. Ye, Y. Zhang, R. T. K. Kwok, J. W. Y. Lam, B. Z. Tang, *J. Am. Chem. Soc.* **2019**, *141*, 5612.

[117] J. Yeow, S. Joshi, R. Chapman, C. Boyer, *Angew. Chem. Int. Ed.* **2018**, *57*, 10102; *Angew. Chem.* **2018**, *130*, 10259.

[118] D. Estupiñán, T. Gegenhuber, J. P. Blinco, C. Barner-Kowollik, L. Barner, *ACS Macro Lett.* **2017**, *6*, 229.

[119] D. Estupiñán, C. Barner-Kowollik, L. Barner, *Angew. Chem. Int. Ed.* **2018**, *57*, 5925; *Angew. Chem.* **2018**, *130*, 6028.

[120] T. S. Fischer, S. Spann, Q. An, B. Luy, M. Tsotsalas, J. P. Blinco, H. Mutlu, C. Barner-Kowollik, *Chem. Sci.* **2018**, *9*, 4696.

[121] J. T. Offenloch, E. Blasco, S. Bastian, C. Barner-Kowollik, H. Mutlu, *Polym. Chem.* **2019**, *10*, 4513.

[122] L. Delafresnaye, F. R. Bloesser, K. B. Kockler, C. W. Schmitt, I. M. Irshadeen, C. Barner-Kowollik, *Chem. Eur. J.* **2020**, *26*, 114 – 127.

[123] A. Roda, *Chemiluminescence and Bioluminescence: Past, Present and Future*, Royal Society of Chemistry, Cambridge, **2011**.

[124] M. Iranifam, *TrAC Trends Anal. Chem.* **2014**, *59*, 156.

[125] M. Vacher, I. Fdez Galván, B.-W. Ding, S. Schramm, R. Berraud-Pache, P. Naumov, N. Ferré, Y.-J. Liu, I. Navizet, D. Roca-Sanjuán, W. J. Baader, R. Lindh, *Chem. Rev.* **2018**, *118*, 6927.

[126] O. Green, T. Eilon, N. Hananya, S. Gutkin, C. R. Bauer, D. Shabat, *ACS Cent. Sci.* **2017**, *3*, 349.

[127] C. Zhao, H. Cui, J. Duan, S. Zhang, J. Lv, *Anal. Chem.* **2018**, *90*, 2201.

[128] L. Mi, Y. Sun, L. Shi, T. Li, *ACS Appl. Mater. Interfaces* **2020**, *12*, 7879.

[129] C. M. Geiselhart, H. Mutlu, P. Tzvetkova, C. Barner-Kowollik, *Polym. Chem.* **2020**, *11*, 4213.

[130] J. X. Xie, W. J. Chen, X. X. Wu, Y. Y. Wu, H. Lin, *Anal. Methods* **2017**, *9*, 974.

[131] N. Hananya, D. Shabat, *ACS Cent. Sci.* **2019**, *5*, 949.

[132] S. Gnaim, O. Green, D. Shabat, *Chem. Commun.* **2018**, *54*, 2073.

[133] L. Delafresnaye, C. W. Schmitt, L. Barner, C. Barner-Kowollik, *Chem. Eur. J.* **2019**, *25*, 12538.

[134] K. B. Kockler, H. Frisch, C. Barner-Kowollik, *Macromol. Rapid Commun.* **2018**, *39*, 1800516.

[135] S. Sadeghi Mohammadi, Z. Vaezi, B. Shojaedin-Givi, H. Naderi-Manesh, *Anal. Chim. Acta* **2019**, *1059*, 113.

[136] M. C. Cabello, O. A. A. El Seoud, W. J. Baader, *J. Photochem. Photobiol. A* **2018**, *367*, 471.

[137] L. C. de Paula Oliveira, I. Gaubeur, P. Dantoni, *J. Lumin.* **2017**, *183*, 418.

[138] K. K. Krzymiński, A. D. Roshal, P. B. Rudnicki-Velasquez, K. Żamojć, *Luminescence* **2019**, *34*, 512.

[139] M. Nakazono, Y. Oshikawa, M. Nakamura, H. Kubota, S. Nanbu, *J. Org. Chem.* **2017**, *82*, 2450.

[140] M. Nakazono, S. Nanbu, *Luminescence* **2018**, *33*, 345.

[141] A. Natrajan, D. Wen, D. Sharpe, *Org. Biomol. Chem.* **2014**, *12*, 3887.

[142] C. M. Geiselhart, C. W. Schmitt, P. Jöckle, H. Mutlu, C. Barner-Kowollik, *Sci. Rep.* **2019**, *9*, 14519.

[143] F. McCapra, D. G. Richardson, Y. C. Chang, *Photochem. Photobiol.* **1965**, *4*, 1111.

[144] Z. Li, B. Zhu, X. Duan, W. Tang, *Anal. Methods* **2019**, *11*, 2763.

[145] A. Giussani, P. Farahani, D. Martínez-Muñoz, M. Lundberg, R. Lindh, D. Roca-Sanjuán, *Chem. Eur. J.* **2019**, *25*, 5202.

[146] W. Gao, C. Wang, K. Muzyka, S. A. Kitte, J. Li, W. Zhang, G. Xu, *Anal. Chem.* **2017**, *89*, 6160.

[147] L. He, Z. W. Peng, Z. W. Jiang, X. Q. Tang, C. Z. Huang, Y. F. Li, *ACS Appl. Mater. Interfaces* **2017**, *9*, 31834.

[148] Y.-S. Borghei, M. Hosseini, M. Khoobi, M. R. Ganjali, *Luminescence* **2017**, *32*, 1045.

[149] K. L. Lin, T. Yang, F. F. Zhang, G. Lei, H. Y. Zou, Y. F. Li, C. Z. Huang, *J. Mater. Chem. B* **2017**, *5*, 7335.

[150] S. Mohammad Beigi, F. Mesgari, M. Hosseini, M. Aghazadeh, M. R. Ganjali, *Anal. Methods* **2019**, *11*, 1346.

[151] Y. Huang, L. Gao, H. Cui, *ACS Appl. Mater. Interfaces* **2018**, *10*, 17040.

[152] L. He, Z. W. Jiang, W. Li, C. M. Li, C. Z. Huang, Y. F. Li, *ACS Appl. Mater. Interfaces* **2018**, *10*, 28868.

[153] W. Cheng, X. Teng, C. Lu, *Anal. Chem.* **2020**, *92*, 5456.

[154] J. Li, X. Zhao, L.-J. Chen, H.-L. Qian, W.-L. Wang, C. Yang, X.-P. Yan, *Anal. Chem.* **2019**, *91*, 13191.

[155] L. Ding, Y. Wu, Y. Duan, S. Yu, F. Yu, J. Wang, Y. Tian, Z. Gao, Z. Wan, L. He, *ACS Sens.* **2020**, *5*, 440.

[156] E. Karshalev, R. Kumar, I. Jeerapan, R. Castillo, I. Campos, J. Wang, *Chem. Mater.* **2018**, *30*, 1593.

[157] J. M. Korde, B. Kandasubramanian, *Ind. Eng. Chem. Res.* **2019**, *58*, 9709.

[158] K. M. Herbert, S. Schrettl, S. J. Rowan, C. Weder, *Macromolecules* **2017**, *50*, 8845.

[159] E. B. Berda, L. F. Deravi, E. J. Foster, Y. Simon, M. M. Thuo, *Macromolecules* **2019**, *52*, 6339.

[160] K. Zheng, Q. Zou, Y. Yang, Y. Mao, J. Zhang, J. Cheng, *Ind. Eng. Chem. Res.* **2018**, *57*, 13283.

[161] Q.-S. Tong, W. Xu, Q.-Y. Huang, Y.-R. Zhang, X.-X. Shi, H. Huang, H.-J. Li, J.-Z. Du, J. Wang, *Polym. Chem.* **2019**, *10*, 656.

[162] J. H. Wieringa, J. Strating, H. Wynberg, W. Adam, *Tetrahedron Lett.* **1972**, *13*, 169.

[163] P. Lechtken, G. Reissenweber, P. Grubmüller, *Tetrahedron Lett.* **1977**, *18*, 2881.

[164] F. McCapra, *J. Chem. Soc. Chem. Commun.* **1977**, 946.

[165] A. Roda, M. Mirasoli, E. Michelini, M. Di Fusco, M. Zangheri, L. Cevenini, B. Roda, P. Simoni, *Biosens. Bioelectron.* **2016**, *76*, 164.

[166] L. A. Andronico, L. Chen, M. Mirasoli, M. Guardigli, A. Quintavalla, M. Lombardo, C. Trombini, D. T. Chiu, A. Roda, *Nanoscale* **2018**, *10*, 14012.

[167] L. A. Andronico, A. Quintavalla, M. Lombardo, M. Mirasoli, M. Guardigli, C. Trombini, A. Roda, *Chem. Eur. J.* **2016**, *22*, 18156.

[168] M. Di Fusco, A. Quintavalla, M. Lombardo, M. Guardigli, M. Mirasoli, C. Trombini, A. Roda, *Anal. Bioanal. Chem.* **2015**, *407*, 1567.

[169] M. Di Fusco, A. Quintavalla, C. Trombini, M. Lombardo, A. Roda, M. Guardigli, M. Mirasoli, *J. Org. Chem.* **2013**, *78*, 11238.

[170] A. Roda, M. Di Fusco, A. Quintavalla, M. Guardigli, M. Mirasoli, M. Lombardo, C. Trombini, *Anal. Chem.* **2012**, *84*, 9913.

[171] D. Cui, J. Li, X. Zhao, K. Pu, R. Zhang, *Adv. Mater.* **2020**, *32*, 1906314.

[172] J. Sun, Z. Hu, S. Zhang, X. Zhang, *ACS Sens.* **2019**, *4*, 87.

[173] N. Hananya, O. Press, A. Das, A. Scomparin, R. Satchi-Fainaro, I. Sagi, D. Shabat, *Chem. Eur. J.* **2019**, *25*, 14679.

[174] S. Gnaim, A. Scomparin, A. Eldar-Boock, C. R. Bauer, R. Satchi-Fainaro, D. Shabat, *Chem. Sci.* **2019**, *10*, 2945.

[175] O. Seven, F. Sozmen, I. Simsek Turan, *Sens. Actuators B* **2017**, *239*, 1318.

[176] M. E. Roth-Konforti, C. R. Bauer, D. Shabat, *Angew. Chem. Int. Ed.* **2017**, *56*, 15633; *Angew. Chem.* **2017**, *129*, 15839.

[177] N. Hananya, D. Shabat, *Angew. Chem. Int. Ed.* **2017**, *56*, 16454; *Angew. Chem.* **2017**, *129*, 16674.

[178] S. Liu, Y. Yuan, J. Li, S. Sun, Y. Chen, *Polym. Chem.* **2020**, *11*, 1877.

[179] Y. Yuan, M. Li, W. Yuan, F. Yang, Y. Chen, *Macromol. Mater. Eng.* **2019**, *304*, 1900056.

[180] C. Yan, F. Yang, M. Wu, Y. Yuan, F. Chen, Y. Chen, *Macromolecules* **2019**, *52*, 9376.

[181] W. Yuan, Y. Yuan, F. Yang, M. Wu, Y. Chen, *Macromolecules* **2018**, *51*, 9019.

[182] J. M. Clough, J. van der Gucht, R. P. Sijbesma, *Macromolecules* **2017**, *50*, 2043.

[183] W. Chen, Y. Yuan, Y. Chen, *ACS Macro Lett.* **2020**, *9*, 438.

[184] Y. Yuan, W. Chen, Z. Ma, Y. Deng, Y. Chen, Y. Chen, W. Hu, *Chem. Sci.* **2019**, *10*, 2206.

[185] J. M. Clough, C. Creton, S. L. Craig, R. P. Sijbesma, *Adv. Funct. Mater.* **2016**, *26*, 9063.

[186] M. Kumar, S. Kumar, *Polym. J.* **2017**, *49*, 85.

[187] Y. Wang, J. Shi, J. Chen, W. Zhu, E. Baranoff, *J. Mater. Chem. C* **2015**, *3*, 7993.

[188] D.-H. Kim, A. Jahn, S.-J. Cho, J. S. Kim, M.-H. Ki, D.-D. Kim, *J. Pharm. Investig.* **2015**, *45*, 1.

[189] D. Wang, S.-Y. Park, I.-K. Kang, *J. Mater. Chem. C* **2015**, *3*, 9038.

[190] J. Deng, W. Liang, J. Fang, *ACS Appl. Mater. Interfaces* **2016**, *8*, 3928.

[191] B. T. Hogan, E. Kovalska, M. F. Craciun, A. Baldycheva, *J. Mater. Chem. C* **2017**, *5*, 11185.

[192] Y.-K. Kim, X. Wang, P. Mondkar, E. Bukusoglu, N. L. Abbott, *Nature* **2018**, *557*, 539.

[193] D. Moldenhauer, J. P. Fuenzalida Werner, C. A. Strassert, F. Gröhn, *Biomacromolecules* **2019**, *20*, 979.

[194] L. Kortekaas, W. R. Browne, *Chem. Soc. Rev.* **2019**, *48*, 3406.

[195] S. Garg, H. Schwartz, M. Kozlowska, A. B. Kanj, K. Müller, W. Wenzel, U. Ruschewitz, L. Heinke, *Angew. Chem. Int. Ed.* **2019**, *58*, 1193; *Angew. Chem.* **2019**, *131*, 1205.

[196] T. Yamaguchi, A. Maity, V. Polshettiwar, M. Ogawa, *Inorg. Chem.* **2018**, *57*, 3671.

[197] Z. Wu, K. Pan, S. Mo, B. Wang, X. Zhao, M. Yin, *ACS Appl. Mater. Interfaces* **2018**, *10*, 30879.

[198] J. Ji, X. Li, T. Wu, F. Feng, *Chem. Sci.* **2018**, *9*, 5816.

[199] A. Abdollahi, K. Sahandi-Zangabad, H. Roghani-Mamaqani, *Langmuir* **2018**, *34*, 13910.

[200] W. Francis, A. Dunne, C. Delaney, L. Florea, D. Diamond, *Sens. Actuators B* **2017**, *250*, 608.

[201] L. Kortekaas, J. Chen, D. Jacquemin, W. R. Browne, *J. Phys. Chem. B* **2018**, *122*, 6423.

[202] Y. Zhang, M. Cao, B. Yuan, T. Guo, W. Zhang, *Polym. Chem.* **2017**, *8*, 7325.

[203] Y. Zhang, S. Chen, M. Pang, W. Zhang, *Polym. Chem.* **2016**, *7*, 6880.

[204] Y. Hao, H. Liu, G. Li, H. Cui, L. Jiang, S. Wang, *ChemPhysChem* **2018**, *19*, 2107.

[205] W. Qiu, P. A. Gurr, G. G. Qiao, *ACS Appl. Mater. Interfaces* **2019**, *11*, 29268.

[206] S. Chen, F. Jiang, Z. Cao, G. Wang, Z.-M. Dang, *Chem. Commun.* **2015**, *51*, 12633.

[207] B. Mondal, A. K. Ghosh, P. S. Mukherjee, *J. Org. Chem.* **2017**, *82*, 7783.

[208] X. Jia, B. Yue, L. Zhou, X. Niu, W. Wu, L. Zhu, *Chem. Commun.* **2020**, *56*, 4336.

[209] Z.-Q. Yao, J. Xu, B. Zou, Z. Hu, K. Wang, Y.-J. Yuan, Y.-P. Chen, R. Feng, J.-B. Xiong, J. Hao, X.-H. Bu, *Angew. Chem. Int. Ed.* **2019**, *58*, 5614; *Angew. Chem.* **2019**, *131*, 5670.

[210] H. Huang, C. Fan, M. Li, H.-L. Nie, F.-B. Wang, H. Wang, R. Wang, J. Xia, X. Zheng, X. Zuo, J. Huang, *ACS Nano* **2020**, *14*, 3747.

[211] W. C. K. Poon, A. T. Brown, S. O. L. Direito, D. J. M. Hodgson, L. Le Nagard, A. Lips, C. E. MacPhee, D. Marenduzzo, J. R. Royer, A. F. Silva, J. H. J. Thijssen, S. Titmuss, *Soft Matter* **2020**, *16*, 8310.

[212] E. V. R. Campos, A. E. S. Pereira, J. L. de Oliveira, L. B. Carvalho, M. Guilger-Casagrande, R. de Lima, L. F. Fraceto, *J. Nanobiotechnol.* **2020**, *18*, 125.

[213] E. Alphandéry, *Bioconjugate Chem.* **2020**, *31*, 1873.

[214] O. Rusin, N. N. St Luce, R. A. Agbaria, J. O. Escobedo, S. Jiang, I. M. Warner, F. B. Dawan, K. Lian, R. M. Strongin, *J. Am. Chem. Soc.* **2004**, *126*, 438.

[215] D. Chen, Y. Feng, *Crit. Rev. Anal. Chem.* **2020**, 1.

[216] M. Tian, Y. Liu, F.-L. Jiang, *Anal. Chem.* **2020**, *92*, 14285.

[217] E. Heyduk, T. Heyduk, *Anal. Biochem.* **2010**, *396*, 298.

[218] B. Li, Q. Yu, Y. Duan, *Crit. Rev. Biotechnol.* **2015**, *35*, 82.

[219] K. Sosnowski, P. Akarapipad, J.-Y. Yoon, *Med. Devices Sensors* **2020**, *3*, e10085.

[220] G. Zhao, W. Yang, F. Li, Z. Deng, Y. Hu, *J. Lumin.* **2020**, *226*, 117506.

[221] C. Han, H. Yang, M. Chen, Q. Su, W. Feng, F. Li, *ACS Appl. Mater. Interfaces* **2015**, *7*, 27968.

[222] Y. Qi, Y. Huang, B. Li, F. Zeng, S. Wu, *Anal. Chem.* **2018**, *90*, 1014.

[223] H.-F. Yin, M.-J. Gao, W.-J. Jiang, Y.-H. Gan, C. Li, Y.-F. Kang, Y.-L. Meng, Z.-H. Xin, *Spectrosc. Lett.* **2020**, *53*, 664–670.

[224] H. Zhu, H. Zhang, C. Liang, C. Liu, P. Jia, Z. Li, Y. Yu, X. Zhang, B. Zhu, W. Sheng, *Analyst* **2019**, *144*, 7010.

[225] D. Cao, Z. Liu, P. Verwilst, S. Koo, P. Jangjili, J. S. Kim, W. Lin, *Chem. Rev.* **2019**, *119*, 10403.

[226] C. Cao, Y. Feng, H. Li, Y. Yang, X. Song, Y. Wang, G. Zhang, W. Dou, W. Liu, *Talanta* **2020**, *219*, 121353.

[227] S. V. Mulay, Y. Kim, M. Choi, D. Y. Lee, J. Choi, Y. Lee, S. Jon, D. G. Churchill, *Anal. Chem.* **2018**, *90*, 2648.

[228] K. Xiong, F. Huo, J. Chao, Y. Zhang, C. Yin, *Anal. Chem.* **2019**, *91*, 1472.

[229] L. Jia, L.-Y. Niu, Q.-Z. Yang, *Anal. Chem.* **2020**, *92*, 10800.

[230] H. Zhang, L. Xu, W. Chen, J. Huang, C. Huang, J. Sheng, X. Song, *ACS Sens.* **2018**, *3*, 2513.

[231] Z. Jia, H.-H. Han, A. C. Sedgwick, G. T. Williams, L. Gwynne, J. T. Brewster, S. D. Bull, A. T. A. Jenkins, X.-P. He, H. Schönherr, J. L. Sessler, T. D. James, *Front. Chem.* **2020**, *8*, 389.

[232] Y. Song, P. Gyarmati, A. C. Araújo, J. Lundeberg, H. Brumer, P. L. Ståhl, *Anal. Chem.* **2014**, *86*, 1575.

[233] L.-H. Xiong, R. Cui, Z.-L. Zhang, X. Yu, Z. Xie, Y.-B. Shi, D.-W. Pang, *ACS Nano* **2014**, *8*, 5116.

[234] Y. Zhu, C. Xu, Y. Wang, Y. Chen, X. Ding, B. Yu, *RSC Adv.* **2017**, *7*, 32632.

[235] D. Li, Y. Fang, X. Zhang, *ACS Appl. Mater. Interfaces* **2020**, *12*, 8989.

[236] Y. Chen, W. Deng, Y. Tan, Q. Xie, *ACS Appl. Mater. Interfaces* **2020**, *12*, 29066.

[237] Y. Ye, L. Zheng, T. Wu, X. Ding, F. Chen, Y. Yuan, G.-C. Fan, Y. Shen, *ACS Appl. Mater. Interfaces* **2020**, *12*, 35626.

[238] L. Yang, W. Deng, C. Cheng, Y. Tan, Q. Xie, S. Yao, *ACS Appl. Mater. Interfaces* **2018**, *10*, 3441.

[239] F. Malvano, R. Pilloton, D. Albanese, *Sensors* **2018**, *18*, 2168.

[240] Z. Jia, I. Sukker, M. Müller, H. Schönherr, *ACS Appl. Mater. Interfaces* **2018**, *10*, 5175.

[241] M.-M. Sadat Ebrahimi, Y. Voss, H. Schönherr, *ACS Appl. Mater. Interfaces* **2015**, *7*, 20190.

[242] A. Gomez, N. S. Miller, I. Smolina, *Anal. Chem.* **2014**, *86*, 11992.

[243] N. Massad-Ivanir, Y. Mirsky, A. Nahor, E. Edrei, L. M. Bonanno-Young, N. Ben Dov, A. Sa'ar, E. Segal, *Analyst* **2014**, *139*, 3885.

[244] S. Ranjbar, M. A. F. Nejad, C. Parolo, S. Shahrokhian, A. Merkoçi, *Anal. Chem.* **2019**, *91*, 14960.

© 2020 The Authors. Angewandte Chemie International Edition published by Wiley-VCH GmbH

These are not the final page numbers! ↗↗

Reviews

Materials Science

C. M. Geiselhart, H. Mutlu,*
C. Barner-Kowollik* ——— ▐▐▐▐–▐▐▐▐

Prevent or Cure—The Unprecedented
Need for Self-Reporting Materials

Are we facing the hard realities imparted
by the limitations of self-healing materi-
als? The answer lies in self-reporting
materials. Prior to any self-healing pro-
cesses, potential system changes along
damages need to be detected and
reported in a visual fashion. This Review
highlights the mechanisms of self-
reporting materials and the challenges
that need to be overcome to enable real-
world applications.